



# Guiding Light in Low-Index Media via Multilayer Waveguides

by

Kristopher J. Rowland

*Supervisors:*

Prof. Tanya M. Monro

Dr Shahraam Afshar Vahid

A thesis submitted in fulfillment of the  
degree of Doctor of Philosophy

in the  
Faculty of Sciences  
School of Chemistry & Physics

December 2010

# Chapter 1

## Introduction

THE year 2010 celebrates the 50<sup>th</sup> anniversary of the laser; light amplification via stimulated emission of radiation enabled the generation of the most spectrally pure and coherent light possible in its day. Now the laser is a commonplace device, responsible for applications from reading and displaying digital media for work or entertainment via compact laser diodes to scientific experimentation and analysis using complex and sophisticated apparatus capable of generating a wide range of light frequencies, pulse lengths, bandwidths and energies. The invention of the laser heralded the field of *photonics*: the study of the behaviour of light and its generation, transmission, modulation, amplification, frequency conversion, and detection [1]. Today, the photon is poised to replace the electron in many of its modern applications, and in some areas has already successfully done so (telecommunications being a prime example - discussed later).

As critical as the generation of light is for technology, so is its manipulation. While the fields of optics and photonics have made many advances by manipulating light using sequences and arrays of mirrors, lenses, crystals, and other optical apparatus, the applications using these techniques are predominantly based upon directing a beam of light, naturally diffracting as it propagates, through various media. These media are usually in a macroscopic and homogeneous form, often termed ‘bulk’ media. While much (arguably, the majority) of the development of optics and photonics owes its existence to application of light propagation through bulk media, the ability to manipulate light beyond its natural tendency to diffract, and doing so on the scale of the light’s wavelength, allows control over it in ways that are otherwise impossible. An established robust and flexible platform for achieving this level of control is by confining light within a *waveguide*.

Optical waveguides are structured optical media that can confine and guide light some distance, from microns to kilometres as the platform permits, without allowing it to diffract as it naturally would in a homogeneous medium. The region to which the light is confined is called the waveguide’s *core*. The core is surrounded by a structure called

the *cladding* which presents a specific refractive index distribution to the light, effectively reflecting some or all of it back into the core. The reflection is the result of coherent scattering from the cladding structure whose form may be anything from a homogeneous medium to a smooth index gradient or a complex, discrete, multi-component structure; the last case being of most interest here. The way in which this reflection occurs, the efficiency with which it happens for various wavelengths, and its relationship with the structure of the cladding is of vital importance for the fundamental behaviour of a given optical waveguide<sup>1</sup>.

## 1.1 Low-index Guiding Waveguides

For this thesis I am interested in types of waveguides in which the core has a refractive index equal to or lower than the lowest index of the cladding structure. Confining light within such waveguides is inherently nontrivial since light naturally ‘prefers’ to propagate within regions of relatively high refractive index. This propensity of light to seek regions of high index is thus the fundamental problem, and hence inherent interest, in coercing light to be guided within a low-index material.

Conventional waveguides typically rely on guiding light within a material of refractive index larger than its surrounds. Such high-index waveguides can be constructed from a wide range of materials. High-index guiding waveguides rely on the *total internal reflection* (discussed in § A.2.1.2) of light incident on the interface between the core and cladding regions<sup>2</sup>. For high-index waveguides with structured claddings, a generalised form of the total internal reflection mechanism can be implied, denoted *index guidance* [2, 3]. When one desires guidance within a material with a lower index than the rest of the waveguide structure, however, index guidance ceases to be a dominant guidance mechanism.

Appropriately designed low-index waveguides are thus of immense importance since they greatly expand the range of materials to which light can be effectively confined and guided within, such as liquids and gases. Such materials hold significant promise for myriad applications once their interaction with confined light, guided over interaction distances unattainable in bulk media, becomes possible.

Low-index waveguides can also be designed with cores made from materials that could otherwise be used as the high-index core feature in another waveguide design. By making

---

<sup>1</sup>Note that this is a simple ray (or more precisely, plane wave) representation of waveguidance. A more physically accurate electromagnetic field ‘mode’ picture is discussed later; this modal description is necessary when diffraction effects become non-negligible.

<sup>2</sup>The term ‘internal’ here refers to the fact that the light must be within the medium of highest refractive index.

such materials the low-index feature, by surrounding them with high-index structure, the guidance mechanisms available to the guided light gives it properties unattainable via index-guiding waveguides, opening up possibilities for applications impossible via index-guiding.

No matter the core material—vacuum, gas, liquid or solid—low-index guidance mechanisms are typically based on resonant interactions with the cladding structure. These resonance phenomena, the structures supporting them and their applications are reviewed in detail in the following section (§ 1.2).

While much of the discussion within can be applied to various waveguide platforms, the focus here is predominantly (but not exclusively) on optical *fibres*: longitudinally invariant waveguides forming a long, hairlike structure. Of particular interest are *microstructured optical fibres* (MOFs): fibres that contain micron-scale structure in the fibre's cross-section. While interesting regimes can be accessed by other platforms, such as planar waveguides, MOFs have proved to be the most versatile in achieving robust and complex transverse waveguide structures over long lengths [2, 3]; a review of the hollow-core versions is presented presently.

The most prevalent variant of a low-index guiding structure is a hollow-core waveguide: a waveguide whose core region consists principally of air<sup>3</sup>. The most simple form of hollow-core fibre (HCF), a simple tube, was first considered by Lord Reyleigh in 1897 [4]; Figure 1.1-*A* qualitatively represents this simple structure. It was only until many decades later, when fabrication techniques and the potential for applications had advanced, that the tube structure was seriously considered for applications requiring the guidance of electromagnetic radiation. In 1964, Marcatali and Schmeltzer [5] published a seminal work on the propagation of light within hollow tubes made of either dielectric or metallic materials. As they discussed, this work came at a time not long after the invention of the laser which, among many other things, ignited great interest in the potential for transporting light for long-distance communication. With various candidates considered for this important application [5–7]—such as sequences of lenses and mirrors for free-space propagation, hollow pipes, and solid-core dielectric waveguides—the hollow waveguide was (after a great amount of research into microwave, millimeter wave and optical waveguides) ultimately not considered as the ideal platform for the task due to issues such as high modal volume, loss, multi-modal dispersion and high bend-loss [7]. It was the latter platform, the ‘dielectric wire’, guiding light in a core of refractive index relatively *higher* than the cladding, which proved to be the most suitable, overcoming many of the shortcomings of the hollow tube approaches. guidance in a high-index dielectric core could confine light at low loss to a much smaller core than possible with

---

<sup>3</sup>The term *air* can be equally substituted with *vacuum* in this context.

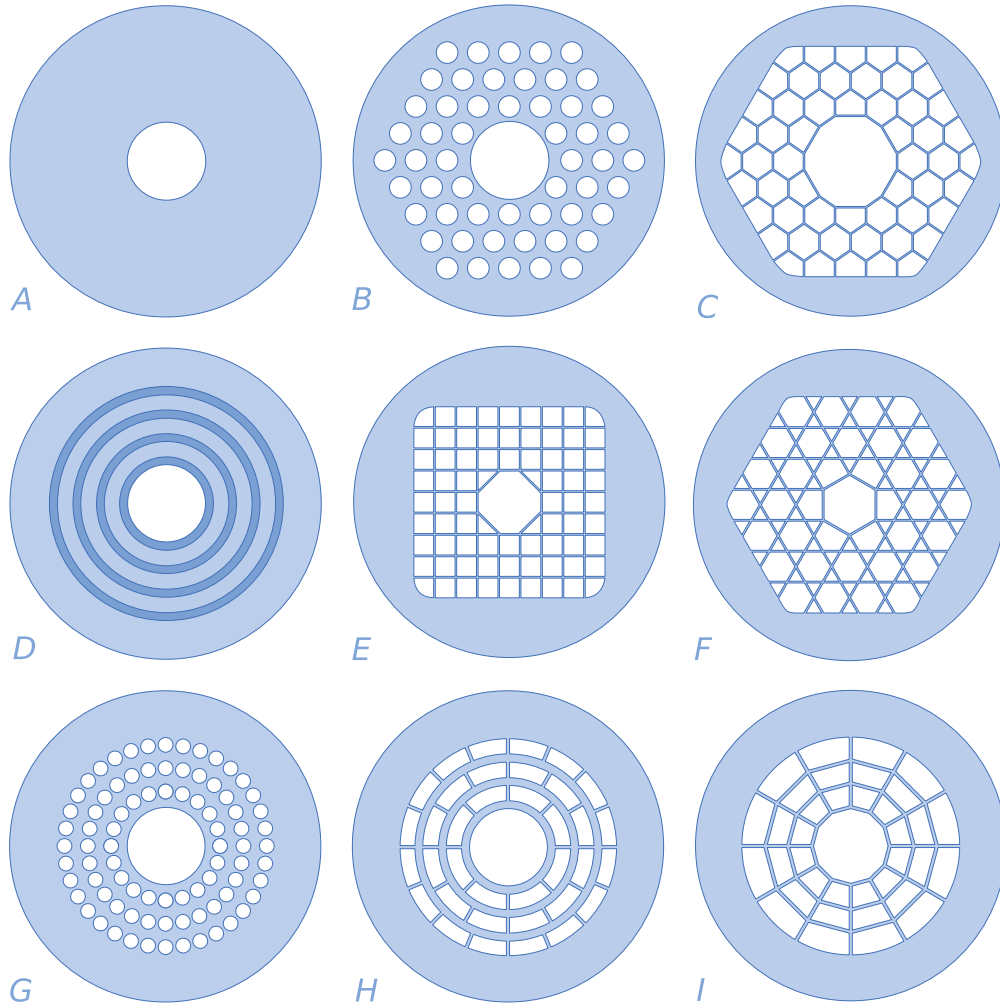


FIGURE 1.1: Qualitative representations of the cross-sectional structures of most of the historical and contemporary hollow core fibres described in the literature. The coloured regions represent a relatively high refractive index substrate whereas white regions represent regions of air or vacuum. *A*: Tube. *B*: Conventional hexagonal-lattice cladding hollow-core MOF. *C*: Honeycomb hollow-core fibre. *D*: Bragg fibre; the darker rings represent a second cladding refractive index higher than the substrate. *E*: Square lattice. *F*: Kagomé lattice. *G*: Average-index Bragg fibre. *H*: Air-Bragg fibre. *I*: Spider-web air-Bragg fibre—a novel waveguide presented in Chapter 5.

a simple hollow tube. This produces fewer modes, reducing the effects of multi-modal dispersion and giving a greater resilience to bend loss, predominantly due to the nature of the total internal reflection mechanism (§ A.2) and great advances made in the reduction of material losses for the silica glass used for the single-mode silica fibres which form a vital ingredient for our global telecommunications infrastructure today [7]. If any more evidence were required for the influence and importance of fibre and waveguide optics in this area, the 2009 Nobel Prize in Physics was awarded to Prof. Charles Kao for, according to the Nobel Foundation, “groundbreaking achievements concerning the transmission of light in fibers for optical communication” [8], which included a significant contribution towards the aforementioned silica material refinement.

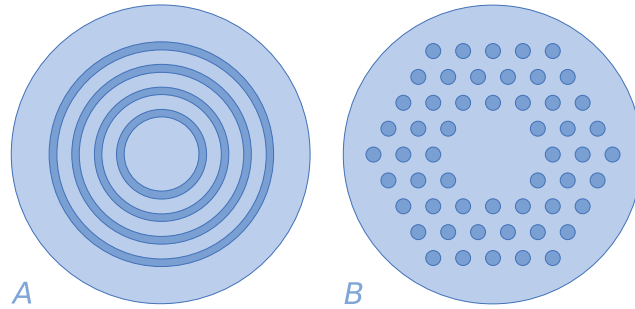


FIGURE 1.2: Qualitative representations of the cross-sectional structures of two level-core fibres. The dark regions represent a relatively high refractive index while the light regions represent a low refractive index. *A*: Level-core Bragg fibre, discussed in detail in Chapter 2. *B*: ARROW fibre.

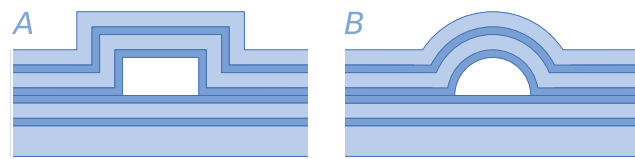


FIGURE 1.3: Qualitative representations of the cross-sectional structures of two Integrated-ARROWs. The dark regions represent a relatively high refractive index while the light regions represent a low refractive index. White regions represent the hollow cores of each. *A*: Rectangular core. *B*: Arch-shaped core.

This history aside, the applications for confining light to a region of *low* refractive index such as air are important and numerous (many discussed in § 1.2), and are applicable to many more applications than just point-to-point transmission. Once the many modern nontrivial waveguide designs are appreciated, the immense potential of guiding light in low-index materials becomes apparent with functionality far superseding a simple tube. Most of the low-index guiding waveguides in question are qualitatively depicted in cross-sectional form in Figs. 1.1, 1.2 and 1.3; their guidance mechanisms, optical behaviour, fabrication and applications as reported in the literature are reviewed in § 1.2.

Often air-guidance is desirable because the confinement of light to air avoids the inherent absorption that arises when it is guided within potentially ‘lossy’ solid materials—materials which, due to their compositional makeup, attenuate light to some degree. In fact, with careful waveguide design, one can produce hollow-core waveguides whose total optical power losses are far less than the substrate material from which the structure is made (examples are discussed in § 1.2). This is unique to hollow-core waveguides since conventional waveguides generally rely on guidance *within* the substrate material which necessarily increases the light overlap with a potentially lossy material. The substrate thus often defines the minimum transmission loss achievable in a waveguide. From this perspective, appropriately designed hollow-core waveguides can break this substrate material loss barrier by guiding light in a region with a lower optical loss, such

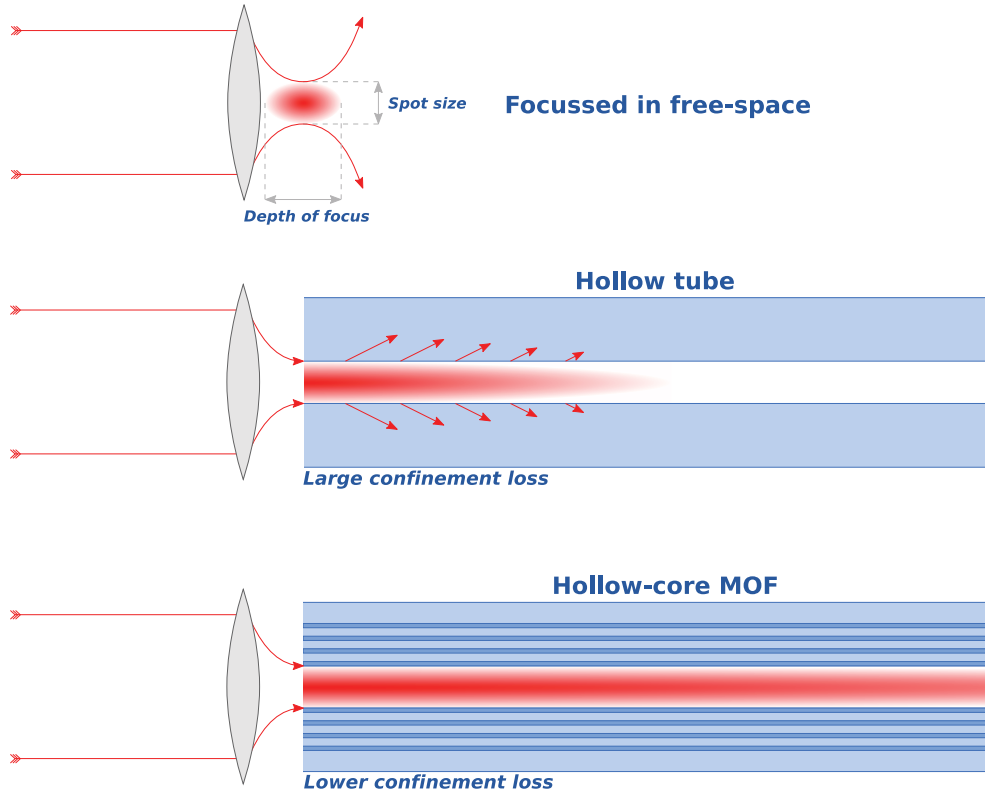


FIGURE 1.4: Comparison between focusing light in free-space, guiding light in a hollow tube, or guiding light in a HC-MOF. Focusing in free-space can produce a high intensity ‘spot’ with a spot size and depth of focus determined by the initial beam width and lens focal length. Guiding light within a tube can confine the light to a beam of diameter about the size of the tube’s bore over an effective length dictated by the relatively large confinement loss of the tube. Guidance within a HC-MOF can confine light at a design wavelength at low loss for much longer effective lengths due to the lower confinement loss possible via coherent scattering from the structured cladding.

as air [2, 3, 9]. This property is important for the creation of optical waveguides for guidance in the mid-to-far infrared spectrum, where many viable waveguide materials have a large optical material loss. This is especially important when high-power delivery is desired such applications as medical laser ablation [10–13] where a lossy substrate material would otherwise succumb to damage were light guided in it directly, owing to the material absorbing excessive power.

Another important concept for many parts of this thesis is the potential to fill a hollow core with gases or liquids. This behaviour offers the possibility of confining light to such materials over interaction lengths unattainable with conventional approaches such as free-space optics, as depicted in Fig. 1.4: an appropriately designed hollow waveguide can enable long light-matter interaction lengths within a hollow or filled low-index core. The free-space analogue can only produce a relatively small interaction region or ‘spot’ due to the diffractive nature of light (Fig. 1.4, top). The purpose of a waveguide is to

combat this diffraction by confining and guiding the light within the waveguide structure. For low-index guidance, a hollow tube achieves this to some degree, but allows light to escape through the high-index cladding region (Fig. 1.4, middle). By adding appropriately designed structure, such as multiple layers, to the cladding surrounding the core, light can be coherently scattered (reflected) back into the core region with much greater efficiency than possible with the plain core/cladding interface of a tube (Fig. 1.4, bottom); comparative analyses between a multilayer MOF and the equivalent simple tube are presented via numerical calculation in later sections, such as § 2. This coherent scattering reflection effect of hollow-core MOFs (with appropriate cladding structure) allows guided light to travel much further at a higher local intensity than possible with a tube or propagation in bulk media.

For example, Gaussian beam optics [14] dictates that in free space a fundamental Gaussian beam's cross-sectional area increases by a factor of 2 when propagating from its focal point, the most tightly focused part of the beam, to its *Rayleigh range*  $z = z_R = \pi w_0^2/\lambda$ , where  $\lambda$  is the wavelength of the light,  $z$  is the propagation distance from the focal point and  $w_0$  is the minimum *waist* of the beam. The waist is measured as the distance  $w$  at which the intensity of the beam drops by  $1/e^2$  from its centre, perpendicular to the axis of propagation; the waist is minimised at the focal point, having value  $w = w_0$ . The 'spot size' of the focused beam is thus  $2w_0$  (the  $1/e^2$ -intensity-based diameter of beam at the focal point), as depicted in Fig. 1.4 (top). This spreading out of the beam reduces the local maximum intensity of the light. The *depth of focus* of the beam can thus, somewhat arbitrarily, be defined as  $l_{d.o.f.} = 2z_R$ , depicted in Fig. 1.4. Many applications of optics require high-intensity light to interact with some material or system over long interaction lengths. One can calculate that the on-axis intensity decreases by 1 dB after propagating about half of the Rayleigh range from the waist; more precisely, a 1 dB loss in axial intensity corresponds to an axial distance from the waist of  $\Delta z \approx 0.509z_R$ . As an example, for a Gaussian light beam of  $\lambda = 1.55 \mu\text{m}$  and  $w_0 = 10 \mu\text{m}$  propagating through air or vacuum, the on-axis intensity decreases by 1 dB after only about  $103 \mu\text{m}$  from the waist.

One can also calculate (*e.g.*, §§ 2.3.1 or A.4.3) the intensity decrease in a tube that maintains a similar spot size. Consider a silica tube ( $n_{\text{silica}} \approx 1.45$ ) with a hollow core diameter of  $40 \mu\text{m}$ ; a core diameter  $4\times$  the waist of the above Gaussian beam would produce guided light with a Gaussian-like intensity profile approximate to that at the waist of the free-space beam. For the same  $1.55 \mu\text{m}$  wavelength, the light in such a tube would travel  $\approx 3.2\text{mm}$  before decreasing in intensity by 1 dB (due to a confinement loss of about  $312.5 \text{ dB/m}$ ); that's about  $30\times$  longer than the Rayleigh range of the free-space equivalent.



In contrast, state of the art hollow core optical fibres can confine such light to similar dimensions in air over almost a *kilometer* before the intensity drops by 1 dB [15–18], making the interaction length many orders of magnitude longer than possible in free space or a simple tube. These comparisons are qualitatively represented in Fig. 1.4.

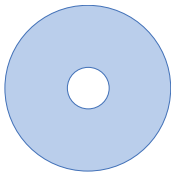
Conventional waveguides require the core region to have a larger refractive index than the cladding so as to exploit total internal reflection (see § A.2). Most low-index materials either have a lower refractive index than the available compatible cladding materials or are in a form incompatible with waveguide fabrication on their own, such as liquids or gases. To circumvent this issue, propagation in the bulk form of a low-index medium (like the free-space propagation example above) is the most simple alternative. With the promise of low-index low-loss waveguidance, however, a significant light-matter overlap can be achieved with such materials over propagation distances unattainable in the bulk material alone. This functionality opens the way for novel applications in sensing [19–22], nonlinear optics [9], microfluidics and particle manipulation [23–29], and waveguide lasers [30, 31], where a long interaction length between material and light is critical.

The most important types of low-index guiding waveguide structures that can be found in the literature today are discussed presently in § 1.2. As mentioned, the perspective will be predominantly toward optical fibres rather than waveguides in general. The simple theoretical explanations of waveguidance discussed here are expanded on in the relevant subsequent chapters throughout and in much more detail in Appendix A. By discussing the various fibre geometries in Figs. 1.1, 1.2 and 1.3 in the sequential manner below, the associated guidance mechanisms can be naturally introduced as the structural and conceptual complexity increases, while also giving a comprehensive review of the literature.

The field of structured optical waveguides, especially fibres, is rapidly evolving, catalysed by the invention of the microstructured optical fibre just before the turn of the millennium. Because of this, a comprehensive overview of the relevant literature, in order to detail the various waveguides and their associated guidance phenomena, fabrication techniques and applications, cannot currently be found in the current literature. Indeed, due to the intimate relationship between the many distinct concepts, the presentation of these details must be careful and considered. This is the intent of the majority of the remainder of this chapter.

## 1.2 Low-index Guiding Waveguides—Review

Figure 1.1 shows qualitative representations of most types of hollow-core microstructured optical fibres reported in the literature today. Each will be discussed here in terms of its guidance mechanisms, fabrication techniques and applications.



**Tube** While a tube (Fig. 1.1-A) is capable of guiding light in low-index media, its simple guidance mechanism is quite restrictive. A tube guides by reflecting light from the single core-cladding interface. Upon each reflection, light is reflected back into the core, propagating down the tube until it is once again reflected. In a ray/plane-wave picture of light, a zig-zag path is traced along the core.

Since the core has a lower refractive index than the cladding, the light can only be *partially* reflected at the interface due to Fresnel reflection, the remaining power being lost to the cladding or ultimately into whatever surrounds the tube. This type of power loss from the core is particular to the confinement mechanism (reflections from the interface in this case), rather than absorption or scattering by the substrate material, say, and is naturally termed *confinement loss* (CL). As the relative size of the core is reduced, the number of reflections per unit length increases, naturally increasing the confinement loss (this is a simple ray picture; a more physical vector wave description is discussed in the following sections). This behaviour means that only large core tubes can be effectively used to efficiently guide light. As discussed in §§ 2.3.1 and A.4.3, this is seen explicitly in the inverse-cube core radius ( $a$ ) dependence and square wavelength ( $\lambda$ ) dependence of confinement loss (CL):  $CL \propto \lambda^2/a^3$ , from Eq. 2.2 (based on [5]).

Cores that are significantly larger than the wavelength of guided light tend to support many *modes*. Each mode represents a specific way of ‘fitting’ the electromagnetic field of light of a specific wavelength within the waveguide. The smaller the core, the fewer ways light can fit, hence it supports fewer modes. Waveguides with only one or a few modes are much more suitable for various applications than those with many modes. For example, exciting multiple modes can broaden an optical pulse since each mode typically travels at a different speed to another, which is often an unwanted effect. Thus, a tube is not an ideal waveguide for few-mode guidance since the use of a small core leads to a correspondingly large confinement loss. Further, such waveguides can not be bent significantly without the loss increasing dramatically [5, 32, 33], providing another obstacle to practical implementation.

To circumvent these kinds of obstacles to low-loss waveguidance in a hollow core, the simple reflections from a single interface as for the tube give way to complex resonance and

interference based interactions with the structured claddings of many modern hollow-core and low-index guiding waveguides. These will be discussed in § 1.2.2 after a brief discussion of some fundamental concepts required for the following sections.

Note that there are many different ways in which to simulate (model) the great number of waveguides reported in the literature, some more appropriate for different structures and regimes than others. Due to the fact that there are so many of them, only those modelling techniques pertinent to the discussion at hand will be described. Those theoretical tools used for the research in the body of this thesis will be discussed in detail when they are required.

### 1.2.1 Waveguidance Concepts

After discussing the simple tube, it is worth introducing some fundamental waveguidance concepts. A thorough theoretical treatment is given in Appendix A, along with a developing dialogue throughout the following chapters. Some fundamentals are abstracted here from these later sections, along with some general comments.

To introduce some important concepts, plane wave approximations to light propagating within a planar waveguide will be considered<sup>4</sup>. More complex models and phenomena are discussed in § 1.2.2 and in much more detail in the following chapters. As discussed in detail in § A.2.1.1 a plane wave travels on a straight path in the direction of its wavevector  $\mathbf{k}$ . Since the whole wave travels in one direction, it can be referred to as a *ray* with its path direction represented as a straight line (the ray). As per Fig. 1.5, rays within either the core layer or cladding region of the planar waveguide in question have wavevector (Eq. A.47)  $\mathbf{k}_i = k_i \hat{\mathbf{k}}_i = n_i k \{\cos \theta_i \hat{\mathbf{x}} + \sin \theta_i \hat{\mathbf{z}}\}$  ( $i = a, b$  for the core or cladding respectively);  $k = 2\pi/\lambda$  is the free space wavenumber,  $\lambda$  is the free space wavelength and  $\theta_i$  is the angle the ray makes with the normal to the interface. As well as  $\mathbf{k}_i$  determining the ray's direction of propagation, it also determines its spatial phase as per the wave's oscillatory factor of  $e^{i(\omega t - \mathbf{k}_i \cdot \mathbf{r})}$  (§ A.2.1.1), where  $\omega$  is the angular frequency of the wave (related to the free space wavelength  $\lambda$  as  $\omega = 2\pi c/\lambda$ ). The phase accumulated by the wave upon the wave propagating a distance  $l$  through a medium of refractive index  $n_i$  is  $\phi = k_i l = n_i k l$ .

Figure 1.5 depicts ray propagation within a planar waveguide with high- or low-index core with respect to the cladding. The layer (the core—refractive index  $n_a$ ) guides light by reflecting the rays from each of the interfaces made with the surrounding medium

<sup>4</sup>More precisely, the waves are assumed to be *locally* plane. Plane waves can strictly only exist in infinite homogeneous media since their equi-phase wavefronts are infinite in extent. In regimes where the effect of the diffraction of light is relatively small, plane waves can often be used as a suitable approximation to components the local electromagnetic field.

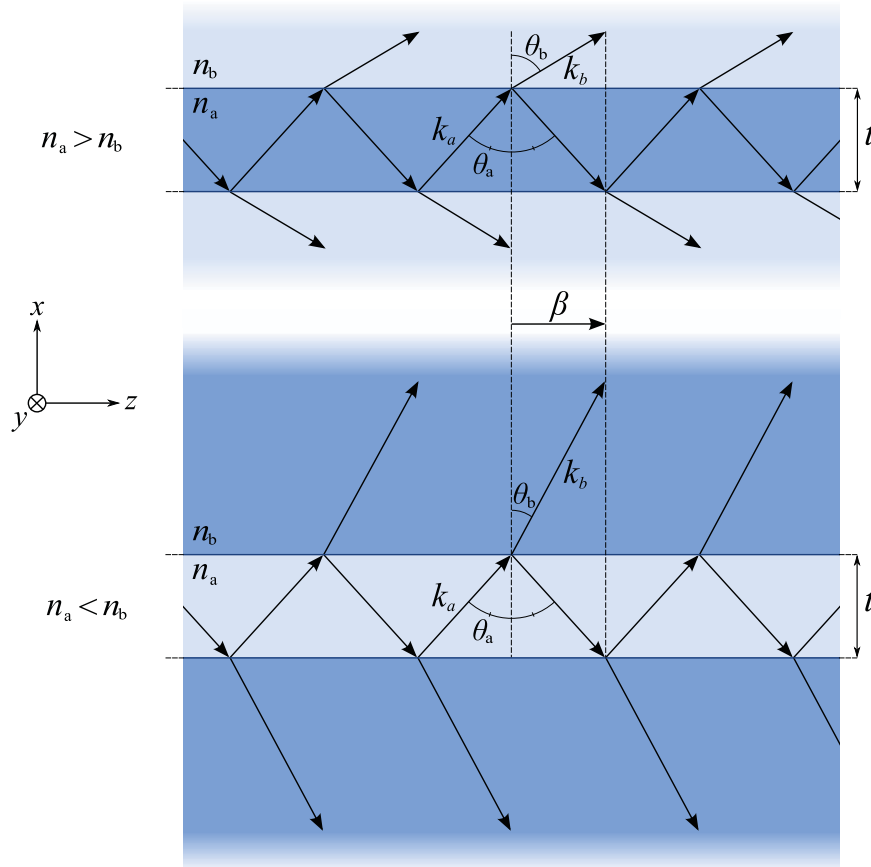


FIGURE 1.5: Ray propagation within planar waveguides with either high- or low-index cores; a duplicate of Fig. A.1. *Top*: A layer with a *higher* core refractive index than the surrounding cladding. *Bottom*: The same waveguide but with a core index *lower* than the surrounding cladding. All vector labels represent amplitudes.

(the cladding—refractive index  $n_a$ ). The reflected rays make the same angle with the interface normal as the incident rays, as per the Law of Reflection (Eq. A.62). Provided the index of refraction of the cladding is different to that of the core (*i.e.*,  $n_a \neq n_b$ ), the light will be reflected back into the layer. Once the light reaches the other side of the core, it is again reflected back toward its centre. This trapping of the light as it travels down the core is referred to as *guidance* or *confinement*. Figure A.1 demonstrates this light-ray guidance concept.

The relative values of the layer and cladding refractive indices greatly influences the type of reflection undergone by the light as it interacts with the interface. If the core index is larger than the cladding index (*i.e.*,  $n_a > n_b$ ), and the angle the guided ray makes with the interfaces is equal to or greater than a critical value (*i.e.*,  $\theta \geq \theta_c$ ), the light will succumb to *total internal reflection* (TIR). In this regime, all light is confined to the core and none can escape into the cladding<sup>5</sup> (§ A.2.1.2 discusses TIR in detail).

<sup>5</sup>Although a portion of the light's field will penetrate into the cladding as an evanescent field, it is bound to the interface and cannot propagate away from the layer. This is discussed in more detail in § A.2.1.2.

If, however, the ray is incident below the critical angle, only a portion of the power of the light is reflected back into the core, with the remainder escaping to the cladding, never to be recaptured. For propagation over a certain distance, then, a certain amount of guided light power will be lost from the guidance region by means purely due to the way the light is confined (such as inherent material losses, say). This effect is known as *confinement loss*. The waveguidance mechanisms behind confinement loss are not always as simple as the example just described, especially when microstructured waveguides are considered (discussed at length in the following § 1.2.2).

Most important for the work considered here, however, light can also be guided within a core of lower refractive index than the surrounding cladding (*i.e.*, when  $n_a < n_b$ ). In this regime, confinement loss occurs for all incidence angles of the guided rays within the core. This is because no TIR regime exists for propagation from a low-index to a high-index medium, hence there will always be some fraction of the light allowed to escape the core guidance region<sup>6</sup>. This is the precise reason why guiding light in low-index media can be troublesome. While some applications can make do with the high transmission losses that come with low-index guidance with a homogeneous cladding, there is a wealth of rich physics and a plethora of unique applications that flow from the various ways in which one can coerce light to be guided within a region with a low refractive index.

While each diagram of Fig. 1.5 represents the same guided longitudinal wavenumber  $\beta$  (the  $\mathbf{k}_a$  vector is the same for each by design—arbitrary but useful here), the transmitted rays differ markedly depending on whether the ray penetrates into a higher or lower refractive index region. Rays propagating from the medium with refractive index  $n_a$  into the medium with index  $n_b$  approach the interface with wave-vector  $k_a$  at an angle  $\theta_a$  to the interface normal and exit with wave-vector  $k_b$  at an angle  $\theta_b$  to the normal, as per the Law of Refraction (Eq A.63). The other possibility is that a fraction (possibly all) all of the light can be reflected from the interface, as discussed, but this regime is not considered here. Figure 1.5 also shows the decomposition of the wave-vectors into Cartesian components: the  $x$ -component  $k_{ix} = \mathbf{k}_i \cdot \hat{\mathbf{x}}$  and the  $z$ -component  $k_{iz} = \beta = \mathbf{k}_i \cdot \hat{\mathbf{z}}$ ; no  $y$ -component exists by the orientation of the  $x$ - $z$ -plane with the plane of incidence here. Integral to much of the following work is that the longitudinal component  $k_{iz}$  is conserved, as will be derived later. *i.e.*, The longitudinal component of the wave-vector has the same value before and after transmission and reflection, so that one may

---

<sup>6</sup>Note that this is a simple ray picture. In a more precise field picture (*e.g.* Appendix A), waves undergoing TIR at a high- to low-index boundary will have an exponentially decaying field amplitude normal to the interface which, if terminated by a high-to low-index boundary, say, *can* be coupled out of the core, inducing a loss. In practice, this cladding region can be made large enough to render such confinement loss negligible. This same tactic of increasing the size of the cladding region can not be used for guidance in low-index media since confinement loss is inherent to guidance within low-index media and not an artifact the premature termination of a TIR evanescent field, say.

set  $k_{az} = k_{bz} = \beta$ ; a direct result of the Law of Refraction, Eq. A.63.  $\beta$  thus becomes an important quantity when considering the confinement of light within a waveguide.

Waveguides support so-called *modes*: rays whose accumulated transverse phase for one round-trip of the slab (traversing the slab twice due to reflection from each interface) is an integer multiple of  $2\pi$ —both propagation and reflection contribute to the phase accumulation, § A.2.1.3. This condition implies that the waves must be *self-consistent* in that their local amplitude is the same upon each round trip. There are only a discrete range of  $\beta$  values (hence ray angles  $\theta_i$ ) that can satisfy this modal condition. It is easy to see that there is a maximum  $\beta$  for which the mode condition is satisfied: a larger value would produce a ray with such a glancing angle  $\theta_a$  (close to parallel with the interface) that it cannot complete a full  $2\pi$  phase cycle in a single round trip. This maximum- $\beta$  mode is referred to as the *fundamental* mode. The discrete modes with smaller values of  $\beta$  are referred to as *higher-order* modes and complete more accumulated  $2\pi$  transverse phase cycles per round trip than the fundamental (larger integer multiples of  $2\pi$  as above). By a similar argument, there are only a finite number of higher-order modes (modes can only have  $0 < \theta_i < \pi/2$ —equivalently  $0 < \beta < k$ ).

Formulation of an arbitrary waveguide system in (the more general) terms of oscillating electromagnetic fields which must satisfy Maxwell's equations (Eqs. A.1 and A.2) shows that this mode description of light guidance appears naturally. In particular, the electromagnetic fields must satisfy the time-harmonic wave equations for inhomogeneous media, derived from Maxwell's equations, § A.1.3. The wave equations require that the solutions have fields whose oscillatory terms are similar to the plane waves above but allowing arbitrary transverse field structure (Eqs. A.21 and A.22)<sup>7</sup>:  $\mathbf{E}(\mathbf{r}_\perp, z) = \mathbf{E}(\mathbf{r}_\perp)e^{i(\omega t - \beta z)}$  (and equivalently for the magnetic field  $\mathbf{H}$ ). These conditions imply that the solutions (the modes) of the waveguide system have invariant oscillations (are harmonic) in both time and the longitudinal spatial dimension. The spatial harmonic condition is equivalent to the self-equivalence of the modes described above for guided rays. The (discrete) modal nature of the solutions is clear when one appreciates that the problem is essentially an eigenvalue problem as per Eqs. A.28 and A.29 (discussed in § A.1.4). The discrete modes have their own values of  $\beta$  and transverse field configurations [ $\mathbf{E}(\mathbf{r}_\perp)$  and  $\mathbf{H}(\mathbf{r}_\perp)$ ]; modes with equal values of  $\beta$  are termed *degenerate*. This wave description of waveguidance is typically used in the body of this work when the calculation of the modal characteristics of various waveguide structures is performed (well beyond the simple case of a planar layer).

Since  $\beta$  is conserved for all types of propagation, in the ray or wave formulation, it is termed the *propagation constant* of a mode. It is useful to define a closely related

<sup>7</sup>The sign convention used for the oscillatory term in certain sections is discussed in § A.1.3 ¶2.

quantity, the *effective refractive index*, denoted  $\tilde{n}$  here. The effective index is related to the propagation constant simply as:

$$\tilde{n} = \frac{\beta}{k} = \frac{\lambda\beta}{2\pi}. \quad (1.1)$$

The consideration of  $\tilde{n}$  as a type of refractive index for a mode can be seen in the way it appears in the wave equations and expressions in § A.1. In general, at least in dielectric media,  $\tilde{n}$  will tend towards the value of the refractive index in which the transverse field is most confined (suggested by the dependence of  $\tilde{n}$  on the fields as per Eq. A.26).

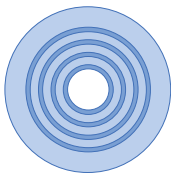
The wave formulation naturally permits the description of confinement loss for the guided modes. When calculating the modes of low-index guiding waveguides, one always finds that the propagation constant is complex:  $\beta \in \mathbb{C}$ . As discussed in § A.1.4 the longitudinal oscillatory field term  $e^{i\beta z}$  produces a decay factor  $e^{-\text{Im}\{\beta\}z}$  for complex  $\beta$ . This field decay is precisely the manifestation of confinement loss inherent in the complex eigenvalues of such modes. As shown in Eq. A.25, this decay leads to a quantitative expression for the confinement loss (loss of power through the transverse structure for axial mode propagation) related to the imaginary part of the propagation constant, or effective index, in units of dB as:

$$\text{CL} = \frac{20}{\ln(10)} \text{Im}\{\beta\} = \frac{20}{\ln(10)} k \text{Im}\{\tilde{n}\}.$$

These considerations are critical for the discussion and analysis within as, according to Corollary A.2, for light guided within a low-index region, TIR cannot occur anywhere within the structure. This has the implication that  $\beta$  (equivalently  $\tilde{n}$ ) will always be complex for such waveguides—all modes will have confinement loss. Such modes are often termed *leaky modes*, for obvious reasons.

### 1.2.2 Effectively 1-D Structures

Waveguide structures based on an effectively one dimensional cladding structure are now reviewed. The term ‘effectively’ is used here since the structures are all either continuously or discretely azimuthally invariant; the cladding structure is composed of either continuous concentric rings or rings made from holes of various shapes. The 1-D nature exists in the radial dimension only.



**Hollow-Core Bragg Fibre** The so-called *Bragg fibre* (Fig. 1.1-D) provides a means of improving confinement loss under hollow-core guidance. The hollow core is surrounded by alternating, radially periodic layers that have thicknesses of the order of the wavelength of the light to be guided. Light impinging on the cladding is thus reflected multiple times from each interface made between the layers and the multiple reflection all interfere with one another. When all reflected light waves return to the core-cladding interface and add *in-phase* (*i.e.*, they are *coherently* scattered), minimal light is lost through the cladding, reducing the confinement loss. However, it is also possible, through varying the wavelength or incidence angle, for the light to add *out of phase* and be predominantly out-coupled through the cladding, substantially increasing the confinement loss. These two opposing conditions see that the transmission spectrum of such a fibre has discrete, periodic, peaks and troughs.

The relative height of the peaks to the troughs increases with increasing numbers of cladding layers, as may be expected; the more layers that exist, the more light that can be coherently reflected, decreasing the minimum confinement loss; Chapter 2 discusses this relationship between the number of layers and confinement loss from a wave/field description of light. This behaviour is essentially that of a one dimensional *photonic crystal* (PhC): a 1-D periodic planar structure; called a *Bragg stack* or *Bragg reflector* in this case of two layer types. In the language of photonic crystals, the conditions of high reflectivity (low confinement loss in-fibre) are said to exist in *photonic bandgaps* [34]; states of light which are denied propagation in the layered structure and hence reflected. This bandgap waveguidance behaviour was discussed earlier with Figs. 1.4 and 1.6.

Bandgap effects can also be observed in periodic structures with higher-dimensionalities, such as a 2-D array of cylinders or 3-D lattice of spheres. In each case, the sub-units (layers, cylinders, spheres, etc.) scatter light in some manner. When the light impinging on the structure has  $(\lambda, \tilde{n})$  within a bandgap, the light is reflected to some degree since propagation in the structure is prohibited. In fact, it is a general principle that the higher the dimensionality, the more scarce the bandgaps [34]. The reason for this is



that there are more ways for light to scatter from photonic crystals with structure in more dimensions, hence a higher likelihood that the scattered light will not add in-phase (not be in a bandgap). 2-D photonic crystal structures will be discussed later for other HC-MOF types.

The concept of the Bragg fibre was first discussed by Melekin and Manenkov in 1968 [3, 35]. A solution to Maxwell’s equations for the 1-D Bragg stack was derived by Yeh, Yariv and Hong in 1977 [36], where the bandgap conditions for out-of-plane propagation were explicitly derived, among many other important results. This analysis was extended to the case of the cylindrical Bragg fibre in 1978 by Yeh, Yariv and Marom [37], later improved upon by others [38–40]; essentially, the plane wave analysis of the 1-D solution in [36] is replaced by a Bessel or Hankel function analysis to accommodate for the fibre’s cylindrical symmetry. Both techniques (for the planar and cylindrical Bragg structures) are covered in Section 2.3 and more thoroughly in Appendix A. The latter work [37] appears to be the first discussion and analysis in the literature of what is now often called a *photonic bandgap fibre* (PBGF), since the guidance mechanism appears to rely on a bandgap effect. For sufficiently large core sizes, the cladding of a Bragg fibre can be approximated by a planar Bragg stack [41–43], a property that is exploited in later sections of this thesis.

Figure 1.6 shows a qualitative representation of bandgap guidance in a Bragg fibre. The ray paths to the left of the figure represent guided light with decreasing (top to bottom images) longitudinal wavenumbers  $\beta$ , and hence decreasing modal effective refractive index  $\tilde{n}$ . Only light with a frequency and longitudinal wavenumber pair  $(\omega, \tilde{n})$  satisfying the cladding layers’ bandgap conditions (the white regions in the figure) can be reflected efficiently and hence guided with low loss. The qualitative bandgap representation in the figure is close to that of the transverse-electric (TE) bandgap of a Bragg fibre cladding (shown in detail in Chapters 2 and 3). In general, modes lying deep within a bandgap exhibit the lowest loss (most efficient reflection from the cladding) and hence maintain a higher guided power. Modes approaching the edge of the bandgap are increasingly permitted to propagate through the cladding since the multiple reflections from the cladding layers become less coherent (less in phase). Modes within the bands (the inverse of the bandgap regions—black regions in the figure) do not support modes at all since light is permitted to efficiently propagate through the cladding. These three scenarios are termed ‘bandgap’, ‘band-edge’ and ‘in-band’ in the figure, respectively.

Cladding bandgaps can exist at other ranges of frequencies, too. The same behaviour holds for modes satisfying the bandgap conditions there, as well, except that they will obviously be of different wavelengths—represented by the different colours of the guided light in Fig. 1.6.

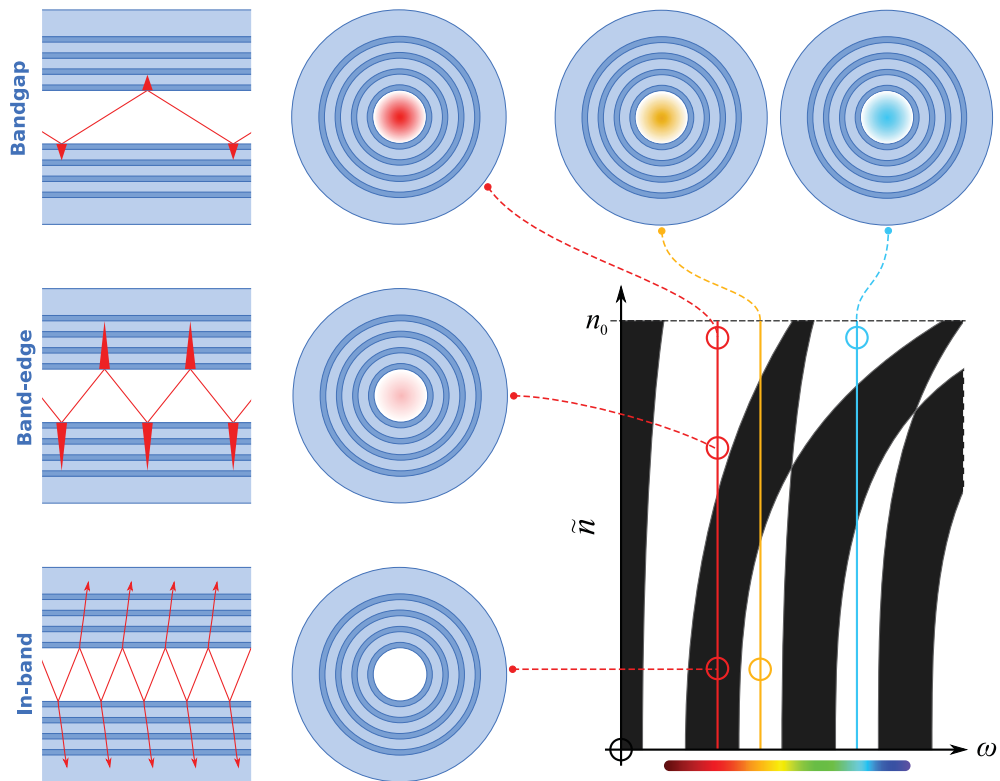


FIGURE 1.6: Simple qualitative representation of bandgap guidance in a Bragg fibre. The ray paths to the left represent guided light with decreasing (top to bottom images) longitudinal wavenumbers  $\beta = k\tilde{n}$ . Only light with a frequency and longitudinal wavenumber pair  $(\omega, \tilde{n})$  satisfying the cladding layers' bandgap condition can be reflected efficiently and hence guided with low loss.

Note that guidance also requires the light's  $(\omega, \tilde{n})$  to satisfy the mode condition on the core as well as the cladding bandgap condition. Thus, the representation of the guided light with lower  $\tilde{n}$  in the end-face views of the figure are rather simplistic here and would realistically exhibit more complex patterns associated with higher-order modes of lower  $\beta$ . Alternatively one can access such lower  $\tilde{n}$  by, when possible, decreasing the core refractive index; discussed in detail in Chapters 3 and 4.

As an aside, as will be shown in detail in Section 3, the bandgap effect isn't the only mechanism that can be attributed to the guidance of a Bragg fibre. Because of similar considerations for other fibres, such as the 2-D ARROW or Kagomé fibres discussed later, the term PBGF quickly leads to confusion when discussing the contemporary literature as a whole. Because of this, here the more general term Hollow-Core Microstructured Optical Fibre (HC-MOF) will be used for any fibre with a hollow core throughout this work, rather than implying a specific guidance mechanism.

Practically, a Bragg fibre requires two layer materials that are sufficiently chemically,

thermally and mechanically compatible. In 1998, Fink et al. [44] demonstrated theoretically and experimentally the viability of an *omnidirectional* reflector based on a Bragg stack made from chemically deposited layers of polystyrene (a polymer) and Tellurium (a chalcogen element). The term omnidirectional refers to the fact that the specific structural configuration reflects most of the incident light for all incidence angles and polarisations (over a limited wavelength range). One year later, the same group demonstrated the fabrication and the predicted bandgap guidance of a large core ( $\sim 1\text{mm}$ ) cylindrical waveguide (essentially a large fibre) whose cladding was an omnidirectional reflector made from polyurethane and Tellurium layers using a similar deposition technique upon a sacrificial silica core which was etched away to produce a hollow core.

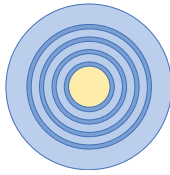
This proof-of-concept paved the way for later demonstrations, again from the same group, of smaller core ( $\sim 100\ \mu\text{m}$ ) Bragg fibres with polyethylsulfonate (PES) and Arsenic-triselenide ( $\text{As}_2\text{Se}_3$ , a chalcogenide glass) layers [41] and polyetherimide (PEI) and  $\text{As}_2\text{Se}_3$  layers [42]; the smaller core sizes achievable were due to the refined fabrication technique employed. The fabrication technique involved depositing layers of the materials onto a planar substrate via physical vapour deposition (PVD) which was then rolled into a cylinder to form a fibre *preform* (a macroscopic version of the target fibre). The preform was then heated and drawn down to fibre in a process very similar to the drawing of other modern fibres [2, 3]: once the preform reaches the critical temperature at which its materials begin to soften, a *drop* forms which is pulled downward due to gravity, leaving behind it a thin strand which forms the fibre (Chapter 5 discusses a fibre drawing process particular to this thesis in much more detail).

These fibres could guide low-loss in the near- to mid-infrared (NIR to MIR) spectrum, wavelengths of about  $0.7\ \mu\text{m}$ – $15\ \mu\text{m}$  (depending on one’s definition), owing to the large core and numerous layers; as discussed above, the more layers, the lower the minimum confinement loss—again, see the results of Chapter 2 for another explanation of this from a field/wave picture. The fibre of [42] demonstrated up to an astounding 35 pairs of layer; keeping the required periodicity over so many layers requires strict fabrication tolerances. The high-reflectivity of the fibre claddings at their design wavelengths means that the optical losses could be reduced orders of magnitude below those of the cladding materials themselves. This permits light to be transmitted through the fibre at very high power without damage to the waveguide; a property which saw the fibre design implemented in precision medical laser delivery devices not long after its demonstration [10, 11].

While most applications only consider a hollow core, Chapter 4 presents an experimental and theoretical analysis I have performed on the spectral properties of Bragg fibres after filling the core with liquids of various refractive indices; the work was a collaboration with Prof. Yoel Fink and one of his students, Alexander Stolyarov, of the Photonic

Bandgap Fibers and Devices Group, Massachusetts Institute of Technology (Cambridge, Massachusetts, US), the group predominantly involved in the above cited research. I presented the results shown in Chapter 4 at the Conference on Lasers and Electro-Optics (CLEO) 2009 in Baltimore, Maryland, US.

The idea of filling the core of a hollow-core Bragg fibre leads to the concept of the next structure.



**Filled-Core Bragg Fibre** A variant on the above type of Bragg fibre is one in which the core is not hollow but filled with a material either during or after fabrication. The bandgap (or antiresonance, Chapter 3) guidance mechanism allows guidance of light in cores of refractive index equal to or lower than the lowest of the cladding layer indices:  $n_{\text{core}} \leq n_0$ . Here I define *level-core* waveguides to be those with a core index *equal to* the lowest cladding index, demonstrated in Fig. 1.2-A, and the more general *depressed-core* waveguides to be those with a core index *equal to or less than* the lowest cladding index (*e.g.*, Fig. 1.1-D, but with a variable core index). A 2-D lattice level-core fibre is discussed later: the ARROW fibre, Fig. 1.2; where a discussion of the unique guidance regime attainable from 1-D and 2-D ARROW fibres is also given.

Before the demonstration of the first hollow-core Bragg fibre discussed above, the first reported fabrication of any Bragg fibre was from Brechet et al. [45–47] in 2000. This fibre’s core was not hollow but solid. The fibre preform was fabricated by using molecular chemical vapour deposition (MCVD) to deposit layers of silica and Germanium-doped silica around a solid rod of slightly Fluoride-doped silica glass, making it a depressed-core waveguide. The preform was then heated and drawn down to fibre in a manner similar to that described above. The resultant fibre had a very small (for a Bragg fibre) core radius of  $6.7 \mu\text{m}$  with layers of about  $1.2 \mu\text{m}$  thickness producing 7 layer pairs. This particular fibre was designed to have a zero-dispersion wavelength about  $1.06 \mu\text{m}$  in order to explore nonlinear effects such as soliton generation and parametric amplification.

Katagiri et al. [48, 49] (in 2004 and 2006, respectively) demonstrated the fabrication of a level-core Bragg fibre by using a sputtering technique to deposit multiple layers of silica and silicon around a prefabricated  $125 \mu\text{m}$  pure silica fibre, producing 8 cladding layer pairs. While silicon is typically an extremely optically lossy material in the visible and NIR, this type of low-index guidance allows light to be guided by, but not contained in, a lossy material, as previously mentioned.

Dupuis et al. [50] demonstrated a similar approach, but used a core and layers made from polymers. To construct the fibre preform, multiple pairs of polystyrene (PS) and polymethyl methacrylate (PMMA) films were wrapped about a large PMMA rod, producing 25 cladding layer pairs. The composite preform was then drawn down to fibre, similarly to the Bragg fibre mentioned above, producing core diameters of  $100\text{--}300\ \mu\text{m}$ . The fact that the cross-section is solid, without a hollow core, makes the scale reduction during drawing much more stable [51] in comparison to the nontrivial dynamics of drawing a similar hollow-core Bragg fibre. In [50], it is demonstrated how by varying the outer diameter of the fibre during the drawing procedure, and hence altering the size of the whole structure (including the layers), the transmission peaks can be shifted through much of the visible spectrum, from green to red. The reason for this is that, up to material dispersion, Maxwell's equations are scale invariant, *i.e.*, as the layers decrease or increase spatially, so do the wavelengths at which the bandgaps sit. This property has even been exploited in the application to 'photonic textiles' [52] in which the fibre is weaved into a fabric whose appearance depends upon the spectral properties of the cladding structure or the transmission out through the cladding of light coupled into the fibres themselves.

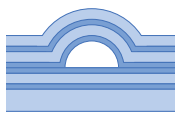
Bookey et al. [53] employed a very similar method to [48] but where a preform was fabricated by depositing cladding layers of silica containing undisclosed dopants (*e.g.*, Germanium) within a jacket and about a core made predominantly of silica. The cladding layers were claimed to have average local refractive indices of about 1.470 and 1.458, whereas the silica core is implied to have an index of about 1.45. This makes the fibre a depressed-core Bragg fibre. The technique employed permitted a relatively small core diameter of about  $11\ \mu\text{m}$ . The small core enables light to be confined to a small area, reducing the number of guided modes and increasing the local power density, opening the possibility of exciting nonlinear optical effects. This behaviour was exploited to demonstrate supercontinuum generation<sup>8</sup> in such a fibre [53]. The complex dispersive and spectral characteristics of such bandgap/antiresonance based fibres, along with such results, enable the possibility of many novel applications for nonlinear optics in low-index media.

While these examples employ solid cores fabricated into the geometry from the start, one can create a filled-core Bragg fibre by filling a hollow-core fibre with liquids or other materials post-fabrication. As discussed above, this forms the main topic of Chapter 4 (presented in Ref. [55]) and is intimately related to Chapter 3.

---

<sup>8</sup>Supercontinuum generation is a complex interplay between various nonlinear optical effects resulting in a significantly broadened spectrum [54]—often used to produce visible white light from a single pump wavelength.

An interesting example of what can be achieved by filling a hollow-core Bragg fibre has been demonstrated by Shapira et al. [30] in which the core of a Bragg fibre very similar to those described in [41, 42] was filled with an organic dye embedded in a copolymer. A significant portion of the dye's fluorescence spectral peak lay within both the longitudinal and transverse bandgaps of the cladding, *i.e.*, the fluorescence light could be confined by being both guided longitudinally along the fibre core *and* (uniquely) confined transversely via a cavity effect; the cladding acted as a mirror to create a resonant cavity perpendicular to the fibre axis. This transverse cavity then formed a laser resonator in which the organic dye acted as a gain medium. The result was *lasing* in the transverse direction, pumped by light propagating longitudinally down the fibre. The device was termed a *surface emitting fibre laser* (SEFL). Because of the cylindrical symmetry of the effective cavity, the emitted light formed a dipole pattern whose orientation depended explicitly on the polarisation of the guided pump light. The applications for such a device range from in-vivo medical imaging to active textiles [30].

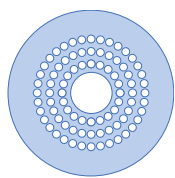


**Integrated-ARROW** Recently there has been significant interest in fabricating a hollow-core Bragg fibre type structure in a planar geometry. Typically called an Integrated Anti-Resonant Reflecting Optical Waveguide (I-ARROW) [28, 56], multiple layers of silicon dioxide and silicon nitride are deposited upon a planar substrate. The core region is created by either the use of a sacrificial medium like polyimide [57], etched out post-fabrication, or by careful ‘crinkling’ of the top layers to reveal a hollow arch-shaped gap [26].

The I-ARROW has been applied to various novel applications, particularly for on-chip microfluidics and particle guidance. Being a planar design with a hollow core it is ideally suited for on-chip microfluidics: the hollow core can act as a channel for pumping through a fluid to interact with the guided light, ideal for sensing [26, 58, 59]. By carefully exciting only a fundamental Gaussian-like mode in the filled waveguide, the ‘optical-tweezer’ radiation pressure effect [60] can be exploited to guide micron scale particles, such as cells or other bio-material, along the waveguide [27, 29]. This application has potential for areas such as sensing, medical diagnostics and on-chip particle sorting.

It is important to note that in the literature, the guidance mechanism of these waveguides is most often attributed to the anti-resonance effect in which light not satisfying the guidance conditions within a individual layers is reflected to some degree back into the core, as opposed to the bandgap mechanism in which light not supported by the entire cladding structure is reflected [61]. Since the geometry of an I-ARROW is conceptually identical to that of a Bragg fibre, one may very well question why the attributed guidance mechanism is most often antiresonance, not bandgap. This question is discussed in detail

in Chapter 3 (and my publication upon which it's based [61]), where a formal unification of the two mechanisms is developed, with many useful analytical tools and conclusions drawn from it.



**Average-Index Bragg Fibre** Figure 1.1-*G* shows a qualitative representation of what is here called an *average-index* Bragg fibre. The concentric rings surrounding the hollow core, instead of being made of a second material, are made up of a finite number of relatively small circular air holes. Note that only one material is required to fabricate the entire structure, rather than the two or more materials for the Bragg structures above; I will refer to such structures as *single-material* HC-MOFs, which describes all but one of the following structures, as well.

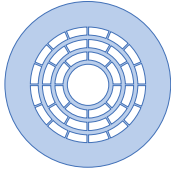
The average-index Bragg fibre was investigated by Argyros et al. [62–65] and demonstrated experimentally by the same group [66, 67] using a polymer substrate, PMMA. The structure was fabricated by machine drilling holes through a cylindrical bulk sample (a *billet*) of PMMA, forming the fibre preform which was then heated and drawn into fibre. The limitation of the drilling preform fabrication technique is that one is restricted to circular inclusions, a drill bit obviously not being able to precisely produce long holes of any other shape.

Numerical simulation [62–65] implies that the guidance mechanism can be interpreted as that of a conventional Bragg fibre, but where the refractive index of the rings of holes is spatially averaged out in some manner to a homogeneous value. This average index must obviously be higher than that of air but lower than that of the substrate material. In this sense, the average-index Bragg fibre is essentially a depressed-core waveguide.

Much like the polymer level-core Bragg fibres discussed above ([50]), Ref. [66] demonstrated the shifting of the transmission spectrum with the global scale of the fibre, again as to expected of a bandgap-type guidance mechanism, but this time in a hollow core.

The fact that only one material was used for the fabrication alleviates the restriction of materials matching. Adding microstructure to a single substrate allows unique freedom to contemplate otherwise unattainable structures and guidance regimes. This is a critical point that is also demonstrated by most of the following waveguides.





**Air-Bragg Fibre** Figure 1.1-*H* demonstrates a structure related to the average-index Bragg fibre, defined here as an *air-Bragg* fibre. Instead of concentric rings of holes, an air-Bragg fibre consists of concentric rings of substrate material supported by thin connective struts. The reasoning behind this design is that it approximates a Bragg cladding consisting of alternating layers of the substrate material and air. Since concentric tubes suspended in air are not mechanically feasible, due to obvious structural issues, the tubes must support each other through the connective struts.

Prior to the my results presented in Chapter 5, the first and only practical demonstration of an air-Bragg fibre was demonstrated by Vienne et al. in 2004 [43, 68]. The fibre was created by constructing a fibre preform from multiple silica tubes and capillaries: three thin-walled tubes were concentrically placed within a larger, thicker, tube which acted as an outer jacket; the voids in between the concentric tubes were filled with many closely packed silica capillaries. The preform was then heated and drawn down to fibre in the usual manner [2, 3], with care taken to preserve the structure. The resultant fibre cross-section was similar to that of Fig. 1.1-*H*, with the capillaries' walls forming the connective struts between the concentric glass rings. For their so-called OD90 fibre, the rings, air gaps and supportive struts had thicknesses  $0.14\ \mu\text{m} - 0.22\ \mu\text{m}$ ,  $2.27\ \mu\text{m} - 2.4\ \mu\text{m}$ , and  $60\text{nm} - 80\text{nm}$ , respectively, with a core diameter of  $\approx 10\ \mu\text{m}$ .

An important observation for the work presented in Chapter 5 is that the cladding rings of this fibre were somewhat distorted from perfect annuli due to the surface tension effect of the softened silica glass during the drawing process. Nonetheless, the large number of connective struts ensured these deformations weren't severe, since the surface tension force was spread more evenly over the rings than it would have been with fewer struts. For an explicit example of this surface tension effect, see the preliminary fabrication trials of Chapter 5.

Experimental testing of the fibre demonstrated that its transmission spectrum was close to what one would expect from a Bragg fibre with alternating silica and air rings. The discrete transmission bands corresponded well to the regions of low confinement loss calculated from a simplified model of the Bragg fibre in which the struts had been neglected and the rings were assumed perfectly cylindrical [43] in spite of the deformations of the rings. Note that this simplified model did not accommodate for an averaging over the refractive index of the air and glass struts in the air rings, as was done for the average-index Bragg fibre above; even if this were done, the effect would be small due to the relative thickness of the struts compared to the space between them (as the agreement with experiment implies). Also, as for the cases mentioned above, varying



the scale of the fibre structure during fabrication also saw the expected scaling of the transmission spectral peaks.

For the work to be shown in Chapter 5, the most important property of the silica air-Bragg fibre demonstrated by [43] is the very low transmission loss measured for so few cladding rings. With only 3 cladding rings, their so-called ‘OD120’ fibre exhibited a transmission loss as low as 1.5 dB/m at  $\lambda = 1.4 \mu\text{m}$ . This is comparable to the losses reported for the conventional Bragg fibres discussed above which are made with many more (tens) of cladding layers and large cores (hundreds of  $\mu\text{m}$ ). The reason for the air-Bragg fibre’s much lower loss is due to the large index contrast of the glass and air layers of the cladding and the fact that the guided modes access the wide transmission bands close to the light line, analysed in detail in Chapter 2. It is this low-loss, wide transmission spectrum behaviour via a relatively simple structure (compared to most other HC-MOF designs) that made the air-Bragg structure an appealing choice for the work presented in Chapter 5.

While the air-Bragg fibre’s observed behaviour agreed with what is expected from the simplified strut-less case, the influence of the struts on the guidance mechanism is also important. There have been various reports [69–73] on the numerical modelling of the modal behaviour of the full air-Bragg structure reported in [43, 68] (or close approximations to it). Thus far, the most promising work [70–72] discusses how the incorporation of struts induces a symmetry breaking that permits the coupling of core modes to modes that propagate within the innermost glass ring itself; these are often called *surface modes*. The type of coupling is demonstrated to be due to *anticrossings*, in which the core mode continuously ‘morphs’ into a surface mode. It was shown [70–72] that the presence of these anticrossings was a likely reason for the observed disruptions in the fibres’ transmission spectra [43]. However, in comparing the confinement loss spectra of the calculated core modes (typically the lowest order modes of each polarisation class), none of the predictions agree with either the experimentally measured transmission spectra or the numerical results of the simplified strut-less model. This point is explored further in § 2.7 where I re-calculate the CL spectra calculations of Foroni et al. [71, 72] of a model of an air-Bragg fibre similar to that of [43].

This disparity between the full numerical model and the simplified model and experimental results implies there is a crucial misunderstanding or missing concept somewhere in the analysis, the origin of which is not clear at this time. The spectral cladding properties of many other popular large and complex transverse structures can be modelled by approximating the cladding as infinitely periodic, permitting a Bloch-wave analysis [34]; similar to the way in which the conventional Bragg fibre cladding can be approximated

by a planar stack, as mention above. This reduces the minimal spatial calculation domain significantly, from the entire fibre cross-section down to a single unit cell. The full air-Bragg structure is not amenable to this type of simplification precisely due to the existence of the connective struts which break the continuous azimuthal symmetry, implying that for as long as one considers the struts the cladding can't be considered as effectively radially periodic. The only way to accurately and precisely model the behaviour of the waveguide is then to model the entire 2-D irreducible structure.

It is conceivable that the numerical methods employed for solving the large and complex structure may be reaching a limit in precision or accuracy in this regime, or at least for the computational resources typically used. However, drawing a conclusion on this possibility would require a thorough review of various numerical techniques and their application to this uniquely nontrivial structure.

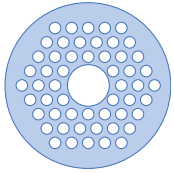
Another possibility is that other guided core modes (beyond just the calculated  $he_{11}$  of [71, 72]) have a significant influence over the transmission spectrum. An explicit example of why this may be necessary is provided in § 2.7 where it is shown how the  $TE_{01}$  mode has a significantly different (broader and lower) CL spectrum which better matches that of the strut-less case.

These technicalities aside, the agreement between the approximate strut-less model and the experimental results imply that the radial thicknesses of the rings are a major determining factor for the waveguide's guidance behaviour. In other words, the interaction of light with the air and glass *rings* in the cladding is the predominant guidance mechanism. This interaction can be considered as bandgap or antiresonant in origin, the distinction becoming less important for large pitch structures as discussed further in § 1.2.3.

Nonetheless, the influence of the connective struts is an important problem, with clear implications for real structures. This issue is investigated from both fabrication and theoretical perspectives in § 2.7 and Chapter 5.

### 1.2.3 2-D Structures

Waveguides based on two dimensional cladding structures are now reviewed. Each waveguide is essentially based on a structure that cannot be classified as effectively 1-D as in the previous section. In most cases, the cladding structure is based on a periodic regular lattice, *e.g.*, hexagonal or square. However, as will be discussed, periodicity isn't required for efficient hollow-core guidance with many of the structures, especially those of large cladding pitch.



**Hexagonal-Lattice Fibre** Figure 1.1-*B* represents a fundamentally different type of hollow-core fibre to those discussed above; one in which the cladding is based on a 2-D, not 1-D, lattice structure. This structure consists of a hollow core surrounded by a cladding consisting of many smaller holes aligned on a periodic 2-D *hexagonal* lattice: each hole is separated from its neighbours by the same distance such that any given three closest neighbour holes lie on the vertices of an equilateral triangle; each single hole is thus surrounded by a ring of holes whose members each lie on the vertices of a hexagon, hence the term ‘hexagonal’—the existence of the equilateral triangle unit sometimes sees the structure also referred to as a *trigonal* lattice. This is a significant departure from the effectively 1-D cladding structures of the Bragg fibres above. Confinement of light to the hollow core using this cladding structure is effective because, like the Bragg fibres above, the cladding structure acts as a photonic crystal.

Two dimensional photonic crystals are well known to exhibit bandgaps for propagation in the transverse plane of the structure [34] (*i.e.*, for propagation directly perpendicular to the holes of the cladding). However, in 1994, Maradudin et al. [74] calculated for the first time that, for a substrate with a hexagonal array of holes, such bandgaps still exist for a large range of incidence angles that lie *out-of-plane*, with some wave-vector component along the invariant longitudinal axis. In 1995 Birks et al. [75] extended this work to calculate the full bandgap spectra for such structures over all incidence angles—now often called a *projected band map*—and made a link with exploiting this out-of-plane bandgap property for waveguidance within a hollow core; light of  $\tilde{n}$  and  $\lambda$  satisfying a bandgap condition (representing a point in a bandgap region of the projected band map) of the 2-D photonic crystal cladding would be reflected back into a low-index core. This type of waveguide is often called a ‘hollow-core photonic crystal fibre’ (HC-PCF), even though the Bragg type fibres above also fall under this nomenclature. Keeping with the convention used in this thesis, here this structure will be referred to as a hexagonal-lattice HC-MOF.

Just as for the 1-D cases above, it is a general principle that the more cladding rings a HC-MOF structure has, the lower the confinement loss will be. Again, as for the 1-D case, this is because an increased number of units in the cladding structure will be able to coherently scatter light back into the core when a bandgap condition is satisfied. This correlation is seen regularly throughout the literature, often via numerical modelling [76–78], and later here in § 3.5.

Important structural measures for a hexagonal lattice of air holes are the *air-filling-factor* and the *air-filling-fraction*. If cladding lattice holes have diameter  $d$  and separation distance  $\Lambda$  (the *pitch*), then the air-filling-factor is defined as the ratio of hole diameter to pitch:  $d/\Lambda$ . The air-filling-fraction is, as the name suggests, the fraction of a cladding unit cell which is occupied by air. It can be shown using some straight-forward geometry that the air-filling-fraction  $A_{\text{air}}$  is related to the air-filling-factor as:  $A_{\text{air}} = \sqrt{3}\pi/6(d/\Lambda)^2$ . It should be noted that this formula is specific only to this geometry of circular holes on a hexagonal (trigonal) lattice.

After considerable effort in inventing and refining a theretofore unknown fabrication technique [2, 3, 79], the first hollow-core microstructured optical fibre (HC-MOF) was demonstrated by Cregan et al. in 1999 [80]. Indeed, this was the first demonstration of a hollow-core microstructured optical fibre, predating even the first demonstrations of the structurally more simple Bragg fibres discussed above [45, 46]. The fabrication technique used employed the close packing of many thin ( $\sim 1\text{mm}$ ) silica capillaries, forming a hexagonal array. Seven capillaries were removed from the centre of the array, leaving a large defect which formed the hollow core of the fibre. This composite preform was then heated and drawn down to fibre in a manner which allowed the holes to remain open without closing, an undesirable effect due to the surface tension of the softened silica glass. This technique is now commonly referred to as the *stack-and-draw* technique. The precise fabrication parameters used ensured that the interstitial air holes remained open during the fibre drawing, almost representing a thick-walled Kagomé structure (Fig. 1.1-*F*), but according to the transmission spectra still convincingly guided via a photonic bandgap effect due to the hexagonal array of holes.

Importantly, it was reported that this fibre guided only a single, gaussian-like, transverse mode, owing to the small 7-cell core. This single-modedness is desirable for any applications requiring well-defined dispersion characteristics and a gaussian-like mode shape such as high-power ultra-short pulse compression and delivery [81]. Also, the guidance of a single mode ensures that the bandgap edges associated with the fundamental mode dictate the transmission spectrum of the fibre, not a superposition of the filtering effect of band edges associated with multiple higher-order modes.

This structure has also been considered for substrate materials of refractive index higher than that of silica ( $n_{\text{Silica}} \approx 1.45$ ) [76, 82, 83]. Refractive indices larger than that of silica exist in so called *soft glasses*: glasses that have a softening temperature lower than that of standard silica glass<sup>9</sup>. Of course, there are many other materials that can exhibit high refractive indices, such as metals or semiconductors, but the ‘glassy’ characteristics (*e.g.*, ability to heat and draw into fibre, relatively low optical attenuation, ability to alter properties via small changes in composition, etc.) of soft glasses make them ideal for fabrication into fibre and their resultant optical properties (*e.g.*, their broad low-loss transmission windows, making them ideal for applications to near- and mid-infrared air-guidance).

Soft glasses are typically made from multiple chemical components in various quantities, important additives being elements such as lead, bismuth and fluorine. For example, the spider-web HC-MOF of Chapter 5 is made from a lead-silicate glass (F2 from Schott Australia Pty. Ltd.). Soft glasses typically have refractive indices higher than that of silica:  $n_{\text{SiO}_2} \approx 1.45$  at  $\lambda = 1550\text{nm}$ , *e.g.*, the aforementioned lead-silicate glass has an index of about 1.6 at the same wavelength. However, there is a subset of soft-glasses that can be made from elements of the chalcogen elemental group, such as tellurium, selenium or sulphur (often coupled with complimentary elements such as germanium, gallium, arsenic and antimony) [84–88]. These *chalcogenide* glasses typically have very large refractive indices. For example, the Bragg fibre used for Chapter 4 uses an arsenic trisulphide ( $\text{As}_2\text{S}_3$ ) glass of index  $\approx 2.6$  for one of the two cladding layer types, very similar to the fibres in [41, 42]. Depending on their composition (their elemental makeup), soft-glasses can produce a continuum of physical, chemical and optical properties, including the refractive index, from the properties of silica through to the chalcogenides (typically thought of as the two extremes of glass compositions) [89, 90].

Pottage et al. [82] demonstrated numerically how new types of bandgaps begin to emerge as the refractive index of a hexagonal HC-MOF substrate is increased. Such bandgaps exist for glass indices from about 1.6 to 3.6 with an optimal bandgap width and depth at about 2.4—much higher than silica. As discussed as a common theme throughout this work, the spectral width of a bandgap determines the lowest loss achievable for a core mode within it (analysed for this very case by Ref. [76]). The depth of a gap refers to its extent in the  $\tilde{n}$  (or equivalently  $\beta$ ) dimension and hence determines the range of effective mode indices the gap can support; the loss of a core mode, as discussed above for the Bragg fibre case, is determined by the distance of a core mode from the gap edges in both the frequency and  $\tilde{n}$  dimensions and thus to the spectral width and

---

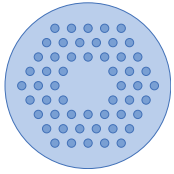
<sup>9</sup>The term ‘soft’ actually refers to the mechanical strength of the glass, *e.g.*, that it can be scratched more easily. This property is typically correlated with its softening temperature, though, so the term can also be used to refer to the lower softening temperature of a glass.

effective index depth of the gap itself. Arguably the most important result of the analysis of Ref. [82] was that the optimal air-filling-fraction of about 60% required to produce such gaps was well below the  $\geq 80\%$  required to produce wide gaps within silica in which bandgap width increases monotonically with air-filling-fraction (which is typically  $> 90\%$ ) [76, 82]. This behaviour reveals the nontrivial properties of 2-D structures with respect to bandgap formation: by changing the substrate refractive index, the bandgap topology can be drastically altered. In contrast, 1-D structures are appealing in this regard: as shown in Chapter 3, 1-D layered structures can produce rich, yet predictable and ordered, bandgap and antiresonance spectra which scale in an analytically manner with structural dimensions and refractive index.

Since the use of a higher substrate index produces gaps requiring a relatively low air-filling-fraction ( $\approx 60\%$ ), one could argue that the fabrication of such fibres has fewer constraints since the shape of the cladding holes remains circular, unlike the honeycomb geometry described later, *i.e.*, the structure would be easier to fabricate owing to its more conventional geometry, not requiring significant inflation, for example (again, see the honeycomb geometry later). In this vein, practical structural parameters for exploiting these gaps were numerically analysed by Pearce et al. and Hu and Menyuk [76, 83]. Pearce et al. [83] numerically investigated the suppression of so-called surface modes in such high-index substrate HC-MOFs. Surface modes are cladding modes that can exist in and about the interface between the cladding structure and the hollow core; discussed in more detail for the honeycomb structure later. Hu and Menyuk [76] later numerically investigated the ideal cladding parameters for fabricating a high-index HC-MOF with a high substrate indices in the range considered by Pottage et al. [82], but expanded the analysis to consider the confinement loss of such waveguides (neglected in [82]). They confirmed the validity of the physically reasonable assumption of [82] that maximising the relative bandgap width also minimised the confinement loss. This concept is well-known for 1-D structures [63], but becomes nontrivial in 2-D structures due to the possibility of light ‘leaking’ through the regions between cladding features.

While these analyses suggest that non-silica high-index substrate hexagonal HC-PCFs are theoretically viable, their fabrication is highly nontrivial. The most promising substrate materials for this task, such as chalcogenide glasses, are very difficult to fabricate into hollow-core MOFs. While much progress has been made into the fabrication of chalcogenide MOFs which guide light within a solid high-index core [84–88, 91–94], the 2-D periodicity of the HC-MOFs like those discussed in [76, 82, 83] must be highly uniform over the cross-section. Small perturbations across the cross-section can destroy bandgap guidance, as demonstrated in [95]. This task is made even more difficult by the analysis of [76] which found that for an optimised HC-MOF with substrate index of 2.6 and air-filling-factor  $d/\Lambda = 0.8$  (air-filling-fraction  $\approx 60\%$ ) the loss is reduced to

below the minimum standard of 1 dB/m only with a minimum of 6 rings of cladding holes (a larger number of features makes maintaining periodicity more difficult). It can only be assumed that these obstacles are the reasons why a high-index soft-glass (*e.g.*, chalcogenide) HC-MOF has not yet been demonstrated. This observation contributed to the decision to focus on 1-D air-Bragg soft-glass HC-MOFs for this thesis, presented in detail in Chapter 5 (and somewhat in § 2.7), as they offer a much simpler geometry and the promise of using far fewer rings for equivalent loss figures and much wider transmission bandwidth.



**(2-D) ARROW Fibre** A variation of the hexagonal-lattice fibre is shown in Figure 1.2-B where the holes in the cladding are replaced with high-index rods and the core is ‘filled-in’ such that it becomes a homogeneous region with the same refractive index as the cladding substrate; it is thus a level-core waveguide.

Much like a lattice of air-holes embedded in a high-index substrate, a lattice of high-index rods embedded in a low-index substrate also produces a full photonic bandgap for out-of-plane propagation [34, 96–98]. Because it is a bandgap effect, it can be exploited to guide light in a low-index core in much the same way as the hollow-core guidance of the above hexagonal HC-MOF. As will be discussed, however, due to its geometry the structure is typically restricted to solid cores, an array of rods suspended in air not being practically amenable to fabrication (at least in the optical regime), much like the idealised air-Bragg discussed above. Making parallels to the air-Bragg fibre, to some extent, the concept of rods (as opposed to rings) suspended in air via interconnecting struts is exhibited by examples of the honeycomb- and square- lattice structures described later.

With the potential for such bandgap behaviour in mind, this level-core structure can also exhibit an important guidance regime for relatively short wavelengths, *i.e.*, for wavelengths sufficiently shorter than the cladding pitch:  $\lambda \ll \Lambda$ . In 2002 Litchinitser et al. [99] demonstrated that in the short wavelength regime, the transmission spectrum of such waveguides is determined predominantly by the size and refractive index of the high-index features in the innermost ring. Using a beam propagation method [99], it was numerically shown that this was due to a strong *anti-resonance* interaction with the innermost features, like that discussed for the I-ARROW above: light precluded from coupling into the features surrounding the core, whether they be solid rings or individual rods, is coherently scattered back into the low-index core region, *i.e.*, light not satisfying the mode conditions of the individual cladding features is reflected back into the core. Ref. [99] showed this only for the effectively 1-D (level-core Bragg type) fibre case, but the effect was theoretically analysed for the 2-D lattice case by White et al. [100].







In the latter work it was explicitly demonstrated that the transmission spectrum was also reasonably insensitive to the relative positions of the high-index cladding features, *e.g.*, rods of the same size but of random position within a ring produced a similar loss spectrum to those with uniform placement. Together with further analysis by Litchinitser et al. [101, 102], it was determined that in the short wavelength regime ( $\lambda \ll \Lambda$ ) the size and shape of the high-index features themselves, and not their relative positions, determine the spectral guidance behaviour of such waveguides. This principle would become synonymous with what is now often called the *antiresonance guidance mechanism* in the field of microstructured waveguides.

As I will show in Chapter 3, this general description of antiresonance breaks down for guidance below the low-index light-line  $\tilde{n} < n_0$ , at least for 1-D layered structures. This is because the mode conditions of the low-index regions become non-negligible in this regime, making the relative positions of the high-index features of critical importance since they define the size of the low-index regions in between.

As it was initially suggested [99], and subsequently analysed and demonstrated (*e.g.*, Refs. [9, 97, 103]), for *longer* wavelengths the relative position and periodicity of the cladding features does become important since the coupling and leakage between them increases; low-loss guidance is then favoured by periodic media producing coherent scattering via bandgap behaviour (*e.g.*, Refs. [34, 96–98] above), requiring a periodic arrangement of structural features. One conclusion from this is that cladding structures with a large pitch tend to exhibit predominantly antiresonance behaviour since the high-index features are sufficiently separated that *coupling between them is reduced*. This is also a phenomenon that is seen in the air-Bragg fibre above and the Kagomé- and square-lattice fibres discussed below, since each structure is of level-core type with high-index cladding inclusions typically separated with a large pitch.

Because most interest in this fibre structure has been borne from its antiresonance guidance behaviour, it is most often termed an ARROW fibre (borrowing the acronym defined above), even though a strictly bandgap regime can also be accessed, but only in the case of a periodic lattice as discussed.

The transition from bandgap to antiresonance guidance regimes via decoupling of the cladding inclusions is summarised, in Fig. 1.7, along with other guidance phenomena to be discussed. The bandgap maps represented in the figure are based on those calculated for an ARROW fibre structure by Birks et al. [104]. The figure represents the effects of increasing the pitch: the tails of the bands in the  $\tilde{n} \geq n_0$  region become relatively thinner, collapsing down upon the trajectory of the mode that would be supported in a single separated cladding rod. This bandgap-to-antiresonance behaviour is described

in various ways by Benabid et al. [9], Yeh and Yariv [36, 37], and Birks et al. [104], discussed further presently.

Closely related to the antiresonance phenomenon is the *photonic tight-binding model* (PTBM). The ARROW fibre geometry was first used to investigate the phenomena on which the PTBM is based. Instead of describing mode behaviour for decoupled cladding features, as the antiresonance model does, the PTBM explicitly includes the effects of coupling by considering the full Bloch modes of a periodic cladding. All representations of the PTBM<sup>10</sup> seek to describe the discrete *edges* of the cladding bandgaps, rather than the full continua of the bands themselves mapped out by all supported Bloch modes.

It was shown by Birks et al. [104] that the Bloch modes of the cladding that were maximally confined to the high- or low-index regions produce mode trajectories that map out the edges of the bandgaps themselves. In fact, they considered approximations to Bloch modes by considering a single cladding inclusion bound by specific boundary conditions imitating a unit cell used to solve for the Bloch modes of an infinite lattice. The similarity with the antiresonance model lies in that each considers regimes in which the cladding light is maximally confined to particular cladding features. The two differ as follows: The antiresonance model approximates the cladding features as independent waveguides, describing only the decoupled regime and able to approximate regions of high transmission loss for core modes close to the low-index light line; the agreement between the cladding rod modes and the band edges breaks down below the light-line, even in the decoupled regime since the modes residing in the low-index portions of the cladding become dominant for regions sufficiently below the light-line [104]; The tight-binding model, on the other hand, considers the cladding as a collection of coupled waveguides (the decoupled antiresonant regime being a special case), describing the bandgap edges themselves, and can hence accurately describe the modal properties of the cladding for any  $\tilde{n}$ .

In short, the PTBM provides a simplified model for determining the band edges of a given bandgap structure, whereas the antiresonance picture provides an (even simpler) model for determining the resonances on and above the low-index light-line ( $\tilde{n} \geq n_0$ ) to which the band edges close upon as the relative pitch increases ( $\Lambda \rightarrow \Lambda \gg \lambda$ ).

Figure 1.7 qualitatively represents these relationships between the decoupled antiresonance regime and the coupled bandgap and PTBM. The figure is ordered into three main sections: bandgap, antiresonance, and Von Neumann Wigner (the latter case is discussed later); PTBM is represented under the bandgap section. The left hand side

<sup>10</sup>Whether they are called a ‘photonic tight-binding model’ or not in the relevant literature is not so important here as their approach is same. PTBM is a convenient and accurate name to use for all approaches here.

of the figure depicts cross sections of two example structures that are commonly associated with bandgap guidance: the 2-D ARROW and honeycomb (discussed in the next section) fibres. Below them, the 2-D ARROW fibre structure with a finite number of cladding rings (3) is focused on. A cross sectional slice is taken, conceptually showing how the field of a core mode (red lines) would be distributed at various positions within a bandgap; being well-confined within the bandgap, as the mode's  $\tilde{n}$  approaches either side of the gap, its (electric<sup>11</sup>) field begins to become more confined in either the low- or high-index cladding regions as appropriate for the particular band edge. In this thesis, this behaviour is theoretically analysed in Chapter 2 for the 1-D equivalent case.

The right hand side of the bandgap section in Fig. 1.7 depicts an infinite lattice approximation to the cladding structure (an infinite number of inclusions with no core defect) and depictions of Bloch modes that may be supported in it. The Bloch modes depicted are examples of those that would be maximally confined to either the high- or low-index regions of the infinite lattice (blue and green lines, respectively), forming the so-called tight-binding Bloch states. The bandgap map for the structure is depicted below this, representing in grey the  $(\omega, \tilde{n})$  regions to which arbitrary Bloch modes are permitted to exist within the structure; the modes defining the edges of the bands are depicted as dark grey lines. The blue and green dotted arrows imply how it is in fact the *tight-binding* Bloch modes that define the band edges, defining the PTBM, closely based on the analysis of [104] as discussed above. Below the bandgap map the transmission spectrum of the considered core mode is depicted; in particular how the band edges themselves define the edges of the transmission peaks.

The antiresonance section of the figure depicts how, as the lattice pitch  $\Lambda$  is increased, the high-index regions begin to decouple from each other such that the Bloch modes themselves approach a degeneracy, the limit of which is the trajectory of the modes supported by a single isolated lattice inclusion, *e.g.*, the modes of a single suspended rod in the 2-D case here. This is the antiresonance phenomenon as discussed above. In particular, the transmission spectrum below the bandgap map represents how the high-loss regions of the core modes are well approximated by the single-inclusion modes (resonances) at cut-off<sup>12</sup> for large relative pitch  $\Lambda \gg \lambda$ . The reason the cut-off points on the  $\tilde{n} = n_0$  light-line satisfy these high-loss regions, rather than the band edges below, is because by increasing  $\Lambda$  the core mode trajectories approach the light-line from below, escaping the effects of such band edges. Note that this happens in spite of the air-type band edges also approaching the light-line in the same manner [104].

<sup>11</sup>The magnetic field could also be considered, but it isn't in order to be consistent with the work of this thesis.

<sup>12</sup>'Cut-off' is the point at which a high-index mode ceases to be truly bound (bound modes for high-index core planar or cylindrical, for example, are bound for  $\tilde{n} \geq n_0$  producing  $\tilde{n} \in \mathbb{R}$  - see Appendix A).

Benabid et al. [9] demonstrated a toy model for considering the tight-binding phenomena in a linear array of high-index rods, similar to the ARROW fibre cladding structure. The work derived a semi-analytic coupled waveguide model for solving for the propagation constants of all modes supported by the rod array. Using this model it was again shown that the edges of the allowed-bands of the waveguide array were defined by the modes confined maximally to either the high- or low-index regions, as required by the PTBM. It was also noted how, for  $\tilde{n} > n_0$ , the supported modes converged upon trajectories common to the modes of a single isolated rod, as required by the antiresonance model discussed above and represented in Fig. 1.7.

In Ref. [9], however, the bands consist of a finite number of modes, rather than a continuum, since a finite number of rods were considered in the array. The more inclusions that are added, the more modes that are supported; an effect that was also analysed for 1-D planar structures much earlier by Yeh and Yariv [36, 37]. The latter work went on to demonstrate how, by continuing this trend of adding elements to the structure, the full continuum Bloch modes (the bands) could evolve from the finite case. The treatment, however, dealt only with modes on and above the low-index light-line ( $\tilde{n} \geq n_0$ ), so while this conclusion is still valid, the region of applicability does not overlap with modes that would be supported in a core defect forming a depressed-core waveguide. On the other hand, the linear rod array model of Ref. [9] considered modes below the low-index line, but corresponds only to 2-D structures consisting of rods.

Chapter 3 presents an extension of this Bloch band evolution concept as presented by Refs. [36] and [37] for 1-D planar multilayer structures for waves *below* the low-index line. A multilayer reflectivity analysis is used as opposed to a modal analysis; the principle is similar for this purpose and at the same time gives significantly more insight into the nature of reflections due to antiresonance. In particular, I demonstrate how the closed form of the reflectance minima can be solved to recover precisely the analytic forms for the resonances (mode conditions) of the layers themselves.

The concept of antiresonance has a deeper history than the relatively recent works discussed above, particularly for 1-D planar structures, but its account is reserved for a thorough treatment in Chapter 3 where the particulars of the various historical theories are required.

The structural simplicity of the ARROW fibre has seen that it can be fabricated by post-processing an existing, well-understood, silica photonic crystal fibre (PCF), namely those with a solid core and hexagonal lattice of holes [2, 3] (just like the ARROW structure presented here but with vacated holes instead of high-index rods). In all cases, the post-processing consists of filling the air holes of the PCF with a material of higher index than the fibre substrate. The most common technique is to fill with a high-index

liquid as discussed by Refs. [102] and [105] and demonstrated experimentally by many works hence [106–111]. Filling with liquid crystals has also been analysed [98] and demonstrated [107, 109, 111, 112].

Liquid-filled ARROW fibres are often demonstrated in a refractive index sensor application as a proof-of-principle for the sensitivity of the transmission spectrum to the properties of the cladding inclusions' refractive index. This is often achieved by altering the index of the filling material by changing its temperature via heating the waveguide; as the temperature of a given liquid changes, its refractive index will also change, depending on its thermal properties (many liquids typically have greater refractive index sensitivities to temperature changes than do solids). When filling with liquid crystals, tuning of the inclusion refractive index can also be achieved by applying a voltage bias across the crystal [112], although the polarisation then becomes important; this technique would make electronic tuning of the resonances possible with a much faster response time than the slower thermal analogue. The application of an ARROW fibre as a refractive index sensor was first discussed by Litchinitser et al. [102, 105] and has since been demonstrated experimentally [106–110, 112].

The shifting of transmission spectra via a change in refractive index is a central theme of Chapters 3 and 4, although it is the core refractive index that is considered, not the cladding inclusion index; a critical distinction.

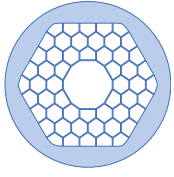
Another variant of the ARROW fibre is one in which the cladding rods are not liquid but solid glass. This can be achieved by either fabricating the fibre using multiple glasses from the beginning [96, 113] or by post-processing by filling the holes with molten soft-glass and allowing it to cool to a solid [114]. The advantage of all-solid ARROW fibres is that issues with filling and sealing liquids in the cladding holes are circumvented and that functionalisation of the filling material can be achieved in ways often inaccessible to liquids, such as doping with rare-earth gain materials.

One such application was considered by Fang et al. [115] in which a PCF's inner rings of holes could be filled in a pattern supporting an 'in-phase supermode' (a distributed multi-peaked fundamental mode which is spatially coherent across the cross-section). It was calculated that if the filled holes contained a gain material such that the supermode produced significant overlap with the material, the light would be amplified significantly (requiring careful tuning of the resonances). Conveniently, the distribution of the coherent supermode profile sees that it forms a Gaussian-like beam profile in the far-field, permitting the local power in the waveguide to be distributed over a larger volume, extending the potential device's damage threshold to some degree.

An interesting approach to all-solid ARROW fibre fabrication was demonstrated by Argyros et al. [116, 117] in which a large-hole prefabricated honeycomb fibre (see below for definition), without a core defect, had many prefabricated multi-mode fibres (of the conventional type: doped-core silica step-index fibres) inserted into its cladding holes. A solid, undoped, rod was inserted into the central hole to create the low-index core. The composite fibre was then drawn again into a composite structure, closing the air regions, creating an ARROW fibre structure consisting of a silica substrate peppered with high-index cladding rods created by the multi-mode fibres' cores. The remarkable feature of these structures was that they produced efficient guidance in the low-index silica core even though the cladding rods only produced an index step of about 1 percent. While such extreme regimes might not have been thought practical from early work on HC-MOFs, it was shown to be consistent with the theory of antiresonant guidance [117].

The ARROW fibre can be seen as a promising platform for applications in which guidance within a solid core of relatively low refractive index is desirable and which exploit the fibres unique dispersion properties, such as nonlinear optical applications [118, 119]. As with most of the structures discussed here, more and more is being learned of ARROW fibres and the antiresonance guidance mechanism, from the particulars of the fundamental guidance mechanism such as the existence of Fano resonances [120] (which has an established history in quantum mechanics) and other concepts [9, 121] to detailed analyses of bend-loss properties [97, 117] (an area of research that is particularly lacking in all literature on low-index guiding waveguides).

For all its convenience with respect to structural simplicity and antiresonant guidance behaviour, the ARROW fibre is restrictive in that the core must always be formed by the substrate material (since it is part of the substrate that hosts the high-index cladding inclusions). This precludes the use of a hollow, or gas- or liquid-filled, core as is possible with the tube, Bragg, and hexagonal lattice fibres above (and all the structures mentioned hereafter). Indeed, were a low-index core to be considered, leaving the higher-index cladding substrate with high-index rods, one finds that the bandgaps terminate at  $\tilde{n}$  not too far below the substrate index [97, 122], as represented in Fig. 1.7. Thus, the only way to achieve a hollow core with a cladding lattice of high-index inclusions is to have the cladding features structurally supported in some way; essentially a feature exhibited by the following fibre types.



**Honeycomb-Lattice Fibre** Closely related to the above hexagonal HC-MOF structure is one which is similar except that it has effectively been significantly inflated, stretching out the structural features to produce a much larger air:glass filling ratio. The resultant cladding structure

is a lattice reminiscent of honeycomb where small solid nodes (where the interstitial air-holes have collapsed) are supported by thin connective struts. Figure 1.1-*C* shows a qualitative representation of this fibre structure. Indeed, after the demonstration of the viability of the 2-D PBG guidance mechanism above [80], this inflated structure quickly became the principal goal for silica based HC-PCFs owing to the fact that the transmission bands increase with an increasing air-filling-factor  $d/\Lambda$  [76, 82].

Official demonstrations of a honeycomb HC-PCF were first reported in conference proceedings by West et al. [123] in 2001 and Venkataraman et al. [124] in 2002, demonstrating guidance in honeycomb HC-MOFs in the NIR spectrum.

The first journal publication for guidance in a similar fibre was reported by Bouwmans et al. in June 2003 [125]. They reported the fabrication and analysis of a silica hollow-core honeycomb fibre, fabricated via the stack-and-draw method using thin silica capillaries. Seven rings of cladding holes were used around a 7-cell core which had a final, elliptical, diameter of about  $6 \mu\text{m} \times 7 \mu\text{m}$ . Guidance was observed in a bandgap extending from about  $800\text{nm} \rightarrow 900\text{nm}$  with a minimum loss of  $180 \text{ dB/km}$  at  $847\text{nm}$ . The cladding pitch was  $\Lambda = 1.94 \mu\text{m}$ , which is, as for many of the following honeycomb fibres, of the order of the central wavelength; the fibre is thus a small-pitch fibre, unlike, say, the Kagomé fibre discussed later (where its importance will become clear).

The final air-filling-fraction of the fibre was over 85%. Since the theoretical maximum air-filling-factor of circular holes on a hexagonal/trigonal lattice is  $A_{\text{air}}^{\text{max}} = \pi/(2\sqrt{3}) \approx 90.7\%$  (found by setting  $d = \Lambda$  in the definition of  $A_{\text{air}}$  above) higher values of  $A_{\text{air}}$  require deformed hole shapes. In reality, the surface tension effects of the softened glass during drawing will begin to deform the holes before this geometrical limit is reached. This is shown in the rounded hexagonal shapes adopted by the holes of the honeycomb-lattice cladding of [125] and all other honeycomb fibres discussed below.

To achieve the higher air-filling-fractions required for larger bandgaps, and hence larger transmission windows and lower losses, one must make the substrate features smaller and thinner [76, 82]; a limit is obviously imposed by the restriction of the amount of inflation possible during the fabrication process and whether or not the struts and nodes can be made smaller and potential issues with fragility of the fine structure during fabrication.

The results of an improved honeycomb HC-MOF were published by Smith et al. later in 2003 [126]. The same stack-and-draw technique was employed using silica capillaries,



also with a 7-cell core. During the fibre drawing stage the outer-diameter was reported as  $125 \mu\text{m}$  with fluctuations of  $\pm 2 \mu\text{m}$  ( $\pm 1.6\%$ ). This suggests that the internal structure is likely to fluctuate by the same relative fraction; a point which is important for the results presented in Chapter 5. The cladding had a hole-to-hole pitch of  $\Lambda = 4.7 \mu\text{m}$  and a very large air-filling-fraction of 94%. The lowest loss of this particular fibre was measured to be 13 dB/km at a wavelength of  $1.5 \mu\text{m}$  with at least two supported core modes.

An important observation of [126] was that the mechanism responsible for the high-loss features discovered *within* the fundamental bandgap was due to coupling of the core mode with modes of the cladding itself. This phenomenon has since been investigated in detail [81, 127–129], finding that these modes reside on the interface of the cladding and core (the core wall) and because of their nature are referred to as *surface modes* (closely related to the case of the air-Bragg fibre discussed above [70, 71]). It has been shown theoretically and experimentally that such surface modes can be suppressed by careful placement of the position and design of the thickness of the core wall such that the periodic cladding is terminated ‘as naturally as possible’ [81, 128, 129]; this property can be anticipated from the understanding that surface modes exist due to the termination of an otherwise periodic structure [34, 81, 128, 129].

As fabrication of the geometry has been consistently optimised and the confinement loss decreases, other loss mechanisms begin to become dominant. One such mechanism is due to light scattering off of so-called *surface capillary waves*: frozen-in ripples on the surface of the inner walls of the fibre due to subtle fluid flow and thermal effects during the drawing process. Roberts et al. [16, 17] demonstrated that by tuning the thickness of the core wall, the intensity of the guided light at the interface can be reduced, limiting the scattering from the frozen-in surface capillary waves. This core wall tuning is closely related to the antiresonance principle discussed above. By exploiting such techniques, the minimum loss of a silica honeycomb HC-MOF has been demonstrated to be as low as 1.2 dB/km [17] and represents the state of the art in terms of low-loss hollow-core waveguidance.

The photonic tight-binding model has been applied to the honeycomb cladding structure, just as for the 2-D ARROW fibre structure above. Couny et al. [122] demonstrated both theoretically and, impressively, experimentally how the tight-binding cladding modes define the edges of the bandgaps and hence spectral transmission peaks of light guided in the honeycomb fibre’s core. The theoretical approach analysed the Bloch modes of an infinite lattice approximation to the cladding. Building on the results of Ref. [104] for the 2-D ARROW fibre structure, the work demonstrated how *three* resonator types dictate the behaviour of the band edges, namely the nodes, struts and holes; the addition of



the strut-type resonators makes the spectral band features of the honeycomb structure more complicated than the 2-D ARROW fibre. Nonetheless, the PTBM was convincingly shown to be valid, the cladding modes bound predominantly to the nodes, struts and holes defining the band edges of the cladding bandgaps in both theory and experiment. The theoretical aspects of this work were expanded upon in [9] discussed above, namely via the PTBM toy-model of coupled rod waveguides, among other observations.

Incidentally, it appears (my having not seen it discussed in the literature) that the reason the honeycomb structure hasn't been observed under or associated with an antiresonance guidance mechanism is precisely because it contains these three resonator features: the nodes struts and holes. The 2-D ARROW can transform from a bandgap to an antiresonance guidance regime because it only effectively has two resonators (the rods and the low-index regions between them) allowing the mode trajectories of each to collapse upon a common dispersion curve (that of a single rod) as the pitch  $\Lambda$  is increased, decoupling adjacent rods and reducing all supported modes to a degeneracy. With an extra resonator feature to consider, such a single degeneracy would not be feasible and, given the complicated interplay between the various tight-binding modes, is the reason a bandgap to antiresonance transition has thus not yet been seen for the honeycomb structure. Nonetheless, given the discovery of the Von Neumann Wigner guidance phenomenon (which doesn't require full bandgaps for core guidance) discussed below, the behaviour of the honeycomb structure in a large-pitch regime warrants further investigation.

Light et al. [130] analysed theoretically and experimentally honeycomb fibre structures which exhibited a higher-order bandgap close in proximity to the lowest order bandgap. They used the PTBM to explain existence of such bandgaps, demonstrating that it was predominantly the node- and strut-type cladding modes that determine the topology and structure of the gaps. In doing so, the structure could easily be optimised to maximise the usable bandwidth of the second gap since the calculation of the tightly bound modes is much quicker than calculating the entire spectrum of Bloch modes. This optimisation procedure led to the fabrication of fibres with two low-loss bandgaps in the NIR spectrum. Such design flexibility can extend the transmission regions such that one could guide both  $\lambda = 1 \mu\text{m}$  light and the whole telecommunications band within  $1.5 - 1.6 \mu\text{m}$ , say, or both 800nm and 633nm simultaneously; this could not be done with previous designs exploiting a single, smaller, fundamental bandgap. The particular fibres fabricated had air-filling-fractions of about 97%, which is well and truly reaching the limits of fabrication of such fibres, evident in the reported deformations of the structure.

While an important result, Ref. [130] again highlights that the hexagonal honeycomb structure, while ideal in its own regime, is rather limited in its scope when other spectral regimes and properties are desired. The Kagomé- and square-lattice structures discussed

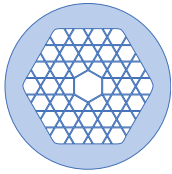
presently provide such alternatives. Chapter 5 (and somewhat § 2.7) focus on a fibre structure I have developed and studied, based not on a 2-D lattice, but on an effectively 1-D (air-Bragg based) geometry.

Due to its well understood properties, the honeycomb HC-MOF has seen many applications. In line with exploiting the hollow core of the fibre, there have been demonstrations of: nonlinear gas lasers [131]; high-power soliton generation [132]; other gas-based nonlinear optics [133–135] (*e.g.*, using Rubidium [134] or Acetylene vapour [135]); electromagnetically induced transparency [136]; gas sensing [137–139] (*e.g.*, saturation absorption spectroscopy with Acetylene [137] and hydrogen-cyanide [138] or carbon dioxide ro-vibrational Raman sensing [139]); and particle guidance [24, 25] in which large particles of polymer can be guided within and along the core of the fibre, with a vision toward biological particle manipulation and sensing. These are some of the most prominent and topical applications, but there are other more commonplace applications such as short and high-power pulse delivery, pulse compression, or spectral filtering.

Further development on this tried and tested silica structure continues, such as the work of Petrovich et al. [140] in which a robustly single-mode honeycomb HC-PCF was numerically and experimentally demonstrated via use of a single-cell core in place of a multi-cell one; the results were comprehensively compared against a 7-cell and a 19-cell core versions. Nonetheless, it appears that a limit has been reached in as far as the loss, usable bandwidth and clean dispersion properties of the silica honeycomb HC-PCF is concerned, wholly due to the choice of cladding geometry and substrate refractive index. The current state of the art, commercially available [18], silica honeycomb fibres exhibit properties such as:

- transmission bandwidths of up to  $\approx 300$  nm,
- transmission losses below  $\approx 10$  dB/km (state-of-the-art down to 1.2 dB/m [17]),
- light/material overlap (fraction of mode power in the substrate) of down to  $< 3\%$ ,

to name a few. However, these properties represent the maximum achievable with the honeycomb structure. For example, wider transmission bands require unreasonably thin cladding features, as discussed in [76, 82]. If a richer variety of guidance regimes are to be accessed, the fundamental structure of the waveguide must be altered, such as the other HC-MOFs discussed already. There are yet more HC-MOF designs, however, which demonstrate nontrivial rich and robust guidance regimes not observed in any of the above structures; these are the fibre structure discussed next.



**Kagomé-Lattice Fibre** One alternate HC-PCF structure is the Kagomé lattice cladding, represented in Figure 1.1-*F*. This structure is very similar to the honeycomb lattice except that the interstitial air holes are kept open during fabrication; sufficient inflation of the structure re-

sults in a lattice of intersecting arrays of struts at an angle of  $2\pi/3$  to each other. The resultant lattice contains sub-units with a star shape<sup>13</sup> made from overlapping two identical equilateral triangles which are rotated by  $2\pi/3$  with respect to each other; it can alternately be viewed as a lattice of hexagons joined only at their apexes, never touching sides, thus leaving interstitial equilateral triangles between each all sides of the adjacent hexagons.

The first report of guidance in such a fibre was by Benabid et al. [141] in 2002. As for the above honeycomb<sup>14</sup> and hexagonal-lattice HC-PCF fibres, this fibre was fabricated via a stack-and-draw process using thin-walled silica capillaries, removing some to make a 7-cell core. In that particular work, the fibre was used as a gas cell which was filled with hydrogen gas and used to demonstrate low-threshold stimulated Raman scattering (SRS) due to the long interaction length offered by the filled waveguide. Indeed, it was calculated, using a reasonable figure of merit [141], that the Kagomé HC-PCF was almost 10,000 times more effective for SRS generation than a simple capillary tube or free-space beam. The ability of this fibre to support the Stokes and anti-Stokes frequencies of the SRS is due to its remarkably wide, low-loss, transmission spectrum (Fig. 3-A of [141]): besides a sharp ‘water’ (OH) absorption peak, the measured loss spectrum demonstrated an unprecedented total transmission loss of less than 3 dB/m over the entire detectable spectral range of 350nm – 1700nm. While not as low-loss as their previously reported hexagonal-lattice HC-PCF [80], the practical transmission window was much wider, easily supporting the multiple generated SRS spectral peaks. The large transmission window can be attributed to the thin  $\sim 500$ nm lattice struts which produce a wide antiresonance response [9]. Further insight into the guidance mechanism and how it differs to that of the hexagonal and honeycomb HC-PCFs was not suggested until some time later [142].

The Kagomé lattice fibre was first explicitly studied as a waveguide in its own right by Couny et al. [143] in 2006 in a work describing a refined fabrication technique for such fibres. Three different fibres were presented, each with a single-cell 7-cell or 19-cell core. The fibres were again fabricated via the stack-and-draw process. It was revealed, however, that in order to maintain the desired structure, the core, cladding and cladding-jacket interface all were pressurised separately, and in all cases the air-filling-fraction was

<sup>13</sup>Sometimes referred to as a ‘Star of David’.

<sup>14</sup>It is interesting to note that the presentation of the first Kagomé-lattice fibre [141] came before the presentation of the first honeycomb-lattice fibre [126].

maintained at  $\lesssim 85\%$  with a strut thickness of  $\approx 500\text{nm} - 700\text{nm}$ . While the guidance mechanism responsible for its unique properties wasn't broached, remarkable properties of the fibre were demonstrated, such as:

- Extremely wide transmission bands:  $> 600\text{nm}$  fundamental bandwidth with low nominal loss  $\approx 1\text{dB/m}$  (19-cell core); even wider in Ref. [141],
- No detectable surface mode interaction over full transmission bands,
- At  $\approx 2\text{ps/nm/km}$ ,  $25\times$  lower dispersion than honeycomb or hexagonal HC-PCF,
- Efficient guidance via the fundamental mode of the single-cell core fibre, even with a large  $\approx 25\ \mu\text{m}$  core diameter.

The fact that the transmission bands are so wide, with an air-filling-fraction of only about 85%, is the first hint that the guidance mechanism is not due to a complete photonic bandgap of the periodic 2-D cladding structure. As discussed, the bandgaps of the honeycomb structure in silica increase with increasing air-filling-fraction; the state-of-the-art honeycomb fibres today can achieve an impressive  $\approx 95\%$  air-filling-fraction but this can only produce a maximal bandwidth of up to  $\approx 300\text{nm}$  [76, 82]. Further, the demonstrated Kagomé lattice had a relatively large pitch of  $\approx 12\ \mu\text{m}$ , compared to the small pitch of  $2\ \mu\text{m}$  of most honeycomb fibres. As discussed in [143], these fabrication challenges, including the suppression of surface modes, of the honeycomb fibre are not an issue for the Kagomé fibre. Coupled with the impressive properties just listed, the Kagomé-lattice fibre represents a fundamentally different type of hollow core fibre providing access to bandwidth and dispersion regimes in which the honeycomb or hexagonal HC-PCF can not operate.

Argyros and Pla [144] reported the fabrication and analysis of a single-cell core Kagomé fibre made from polymer (PMMA) via a stack-and-draw process, exhibiting similar broad-band transmission behaviour as for the silica versions above. The significance of the demonstration was that it was the first hollow-core polymer fibre with demonstrable guidance. Moreover, it exhibited guidance in the infrared spectral region, where polymers are typically very lossy [144], thus circumventing the inherent high losses of the substrate (much like the Bragg fibre examples discussed above, *e.g.*, Ref. [41, 42]).

The work was also the first to explicitly analyse the guidance mechanism of the Kagomé structure. It was found that the cladding actually *doesn't exhibit a full photonic bandgap* as do the honeycomb and hexagonal structures discussed above. A density-of-states map of an infinite-lattice version of the cladding structure is thus non-zero *everywhere* [142, 145], representing a uninterrupted continuum of Bloch states on the lattice. The explanation for the tenacious guidance was attributed to a combination of well-separated propagation constants between the core and cladding modes and, when this isn't the case, a small field overlap between the core and cladding modes. With separated propagation constants and poor field overlap, the core and cladding modes have

very low coupling between each other [146]. The cladding modes were also identified as being either predominantly confined to the high-index struts of the lattice or to the low-index holes.

This high- and low-index mode/structure identification was numerically explored further by Pearce et al. [145] in which the continuum cladding band-map was shown to exhibit strong features of both modes confined to the struts *and* modes confined to the holes; a theme investigated in detail for 1-D structures in Chapter 3. The work also went on to demonstrate the strong similarities between the Kagomé-lattice guidance and that of claddings constructed from concentric shapes (hexagons or circles) approximating the Kagomé structure without connective struts; very similar to the idealised air-Bragg fibre structure discussed above [43, 147], discussed in more detail in Chapter 2. The high-loss peaks for these concentric ring approximations were, as one may expect from the behaviour of the air-Bragg fibre [43, 147], attributed to resonances with the high-index rings. Since the core-guided modes satisfied conditions so close to the ‘air-line’ [145] (their propagation constants were close to those of plane waves in a free space vacuum), the resonances of the low-index hole modes had a negligible effect on the confinement loss spectrum of the core mode; a point which is explained in detail for the case of an arbitrary 1-D Bragg cladding in Chapter 3. Calculations of the equivalent Kagomé structure reveal that the positions of the corresponding high-loss regions are aligned with those of the ring-based analogues, implying that the high-index struts are the dominant resonance feature for both the full Kagomé and ring structures. For narrow loss peaks, then, one requires cladding features of equal thickness throughout, especially around the core; this later point is quite different to the requirement of the honeycomb-cladding fibre which requires the core wall to be tuned so as to suppress surface modes capable of inducing coupling losses with the core modes, as discussed above.

A critical conclusion of the Pearce et al. work [145] was that the addition of extra cladding unit cells (2 rings to 4 rings) had a negligible effect on decreasing the modal confinement loss, maintaining it at the order of 1 dB/m – 10 dB/m for the main transmission region analysed. This is at direct odds with the behaviour of the simplified concentric hexagonal ring model, whose loss decreased by over two orders of magnitude to  $\approx 0.5$  dB/m by adding one extra ring to a single-ring model [145]. It was argued that this discrepancy in behaviour was due to the connective struts of the Kagomé structure dominantly coupling light through the cladding; possible due to the non-existence of any full bandgaps, *i.e.*, the resonances of the struts, as for the concentric ring case, confine the light via antiresonance, but this confinement is interrupted by efficient out-coupling through the lattice struts connecting the concentric rings.

This concept possibly explains the results of the work of Eijkelenborg et al. [148] in which it was shown how a 2-ring polycarbonate Kagomé type HC-MOF exhibited a minimum confinement loss of  $\approx 3.1$  dB/m at  $\lambda = 1550$ nm using rings of average thickness 640nm and a 61  $\mu$ m core, similar to most Kagomé fibres (as above) with many more than just 2 rings.

Indeed, similarly low losses have also been demonstrated by Gerome et al. [149] in a silica HC-MOF with only a *single* ring; the one 340nm ring is sufficient to provide antiresonance with the light in the 35  $\mu$ m core to produce confinement losses as low as 0.2 dB/m at  $\lambda \approx 600$ nm.

Given the above argument of strut-limited confinement loss, one could argue that by removing as many struts as possible, leaving the concentric rings intact (as simulated in [145]), one may considerably reduce the modal confinement loss by limiting the leakage through the struts. This is not suggested as a fabrication possibility in works such as [145, 148]; to the best of my knowledge, this idea, and progress towards its execution, is unique to this thesis. Indeed, this is precisely the type of structure, represented in Fig. 1.1-I, that I have fabricated for this research and is discussed in Chapter 5. Note that in relaxing the structure to one of concentric polygons in this manner, the number of vertices in each ring need not be restricted to the 6 of the Kagomé lattice rings, but may be greater or lesser as desired; just one of the increased degrees of freedom of the new structure.

Couny et al. [142] discussed the guidance mechanism of the Kagomé fibre in more detail. In it, it was suggested that the bound modes that exist in the core of the Kagomé fibre are akin to the discrete energy levels that may exist in a continuum of states as described by Von Neumann and Wigner in 1929 [150], shortly after the invention of quantum mechanics, in their work “Uber merkwürdige diskrete Eigenwerte” (which loosely translates as “On strange/anomalous discrete eigenvalues”), and later expanded on by Stillinger et al. [151]. The Von Neumann Wigner (VNW) phenomenon relates to the existence of a discrete set of eigenstates that occupy energies above the walls of a spatially oscillating quantum potential, in spite of the existence of a continuum of lower-energy background states. VNW states were experimentally measured by Capasso et al. [152] as excited electronic states in a stratified semiconductor heterostructure. This is directly analogous to the behaviour of light within the Kagomé fibre structure: Refs. [142, 144, 145] show the continuum<sup>15</sup> of cladding modes that exist in the structure, never producing a

<sup>15</sup>Technically, Fig. S1 of the supplementary material of Ref. [142] and Fig. 1 b) of Ref. [145] are the only true representations of the continuum, showing a density-of-states map of an infinite lattice. The other references demonstrate calculations of the modes for a necessarily spatially finite representation of the full fibre structure, hence the continuum of modes is reduced to a discrete set of cladding modes; this continuum-to-discrete behaviour under infinite-to-truncated regimes is expected from the tight-binding analysis of, say, [9, 36, 153]. Nonetheless, the absence of a full bandgap is clear in all cases.

bandgap. To push the analogy further, the fact that the high-loss regions of core-modes in the Kagomé fibre exist close to the resonance conditions of the struts (discussed above, and explicitly in Refs. [9, 142]) is very similar to the coherent diffractive wavefunction interference effect responsible for the quantum VNW phenomenon [150, 152]. The VNW phenomenon is in agreement, then, with the concept of the co-existence of core and cladding states which don't interact due to low inter-mode coupling, as described above [9, 144].

A comparison of the VNW-enabled antiresonance guidance behaviour of waveguides such as the Kagomé fibre is qualitatively represented in Fig. 1.7. Gaps in the cladding band map no longer exist for such waveguide structures, allowing the core and cladding modes to occupy the same regions in the band map. Regardless of their coexistence coupling between the core and cladding modes has very low efficiency due to their poor overlap arising from the large pitch of the structure. This allows the core mode to propagate at low loss with minimal interaction with the cladding modes in the absence of a true cladding bandgap. The transmission spectra of the core modes is dominated by the antiresonant interaction of the core mode fields with the surrounding cladding struts, just as described for all of the antiresonance phenomena above. It is important to keep distinct the concepts of modal resonance and inter-mode coupling; the resonance of the core modes with the structure does not require interaction with the cladding modes—although the existence of the cladding modes is deeply related to the existence of the resonances. This is explored in various ways in this thesis, numerically for effectively 1-D §§ 2.4.2 and analytically for purely 1-D 3.5 structures.

Von Neumann Wigner guidance and the dominance of antiresonance within these large-pitch structures implies that the cladding structure need not be periodic, as discussed for the ARROW fibre above. Examples of aperiodic square-based cladding lattices are discussed below. There are more extreme demonstrations of this permissible aperiodicity, however. Skibina et al. [154] and Bethge et al. [155] demonstrated a silica HC-MOF whose cladding lattice resembled a Kagomé pattern which was *radially chirped* with the lattice pitch increasing from the inner to the outer rings. Beyond antiresonant hollow-core guidance, Ref. [154] demonstrated experimentally how such a structure produces lower modal dispersion than currently demonstrated Kagomé fibres; the argument being that the chirped cladding helped smooth out sharp resonances, as numerically investigated<sup>16</sup> in Ref. [155].

---

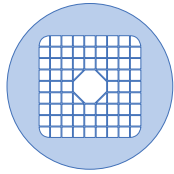
<sup>16</sup>Although it was not explained how or why the structural convolution technique of Ref. [154] works, except that it produced numerical results closer to experiment than the untreated data.



An even more extreme demonstration of the permissibility of aperiodicity has been demonstrated by Konorov et al. [156] in which a *random* large-pitch thin-strut HC-MOF was demonstrated. Few details of the hollow-core guidance properties of that particular fibre were discussed, but observable hollow-core guidance was reported. By permitting such a variety of cross-sectional structures which support robust and rich guidance regimes, large-pitch HC-MOFs and their many designs exploiting VNW and antiresonant guidance will surely represent the next generation of state-of-the-art low-index guiding waveguides.

There have been many other application of the Kagomé fibre, the most prominent of which exploit its broadband low-loss guidance behaviour. Of particular note is the work of Couny et al. [142]: by filling a Kagomé fibre with hydrogen gas, a stimulated Raman scattering (SRS) frequency comb spanning over *three octaves* (from 325nm to 2500nm) was generated, of which all frequency components were efficiently guided in the fibre. The effect was demonstrated at powers much lower than those used in other techniques, down to six orders of magnitude lower in peak power, possible because of the long interaction length and low broadband loss offered by the Kagomé fibre structure. The bandwidth spanned by the frequency comb was almost 1THz, approaching the UV to IR span required for ultra-short (potentially attosecond) pulse generation and guidance [9] and similar applications, something that is impossible using the limited bandwidth [82] of other established hollow waveguides such as the honeycomb fibre.

Many other Kagomé fibre applications have been demonstrated such as stimulated Raman scattering in hydrogen gas filled fibres [141] (and with enhanced efficiency from Bragg gratings written into the fibre structure [157]), leading to the generation of the aforementioned three-octave Raman-induced frequency combs [9, 142] (pointing a way toward fibre based low-power ‘atto-science’ [142]), robust integrated HC-MOF gas-cells [131], and particle guidance [23] in which particles of polystyrene were guided within and along the core of the fibre (with a vision toward applications to biological particle manipulation and sensing, say). With the advent of similar VNW/antiresonance guiding fibres (including the spider-web fibre I present in Chapter § 5) the applications of the robust and rich guidance regimes of this type of fibre can only increase in number and importance.



**Square-Lattice Fibre** The square lattice HC-MOF depicted in Figure 1.1-*E* is a variation on the honeycomb and Kagomé structures in that it is based on an array of thin struts, but this time arranged on a lattice whose unit cells are squares. This structure is interesting in that it can exhibit both bandgap behaviour [158] and antiresonance behaviour [159], the latter possible due to a VNW effect as for the Kagome lattice [9, 142, 144, 145].

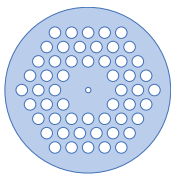
Poletti and Richardson [158] numerically investigated the guidance behaviour of a HC-PCF based on a square lattice of thin struts whose intersection points form nodes; *i.e.*, no sharp corners. An example of the pitch of the cladding unit cells for guidance about  $\lambda = 1540\text{nm}$  was  $\Lambda = 2.8 \mu\text{m}$ ; close to the wavelength. They demonstrate how such a structure can produce a fundamental bandgap 20% wider than a honeycomb structure at the expense of a greater number of unit cells rings required to reduce the confinement loss. Using a 9-cell core, the considered fibre structure is effectively single-moded with the first higher-order-mode (HOM) having CL 4 orders of magnitude higher than the fundamental mode; due to the HOM being pushed out of the bandgap, an effect which is discussed for 1-D structures in Chapter 2. The demonstrated cladding bandgap was shown to be predominantly sensitive to the radius of curvature of the nodes, which dictates their size; larger radii of curvature produce larger nodes. It was shown that as the size of the nodes was altered, the bandgap size and position shifted accordingly; while not mentioned in the work, this is again in accordance with the photonic tight-binding model [9, 122] in which the Bloch modes bound predominantly to the nodes would dictate the bandgap structure (similarly to the antiresonance behaviour of the ARROW cladding rods discussed above).

Argyros et al. [159] demonstrated a square-lattice hollow-core fibre using a polymer substrate (PMMA). Couny et al. [160] demonstrated a very similar structure using a silica substrate. In each case, the fibre was made via a stack-and-draw process in which the polymer or silica capillaries were stacked in a square array and drawn such that the interstitial air-holes between the capillaries are kept open, becoming equal in size to the capillaries themselves as the fibre is drawn under tension with the walls of the capillaries stretching until they are straightened to form the hatched pattern of the square lattice. Importantly, this technique sees that the nodes formed at the junctions of the struts are almost non-existent (*i.e.*, have a very small radius of curvature). In each work [159, 160], the core is made by removing a single capillary from the centre of the structure, with [160] also fabricating a zero-cell core variant by not removing any capillaries and inflating the central lattice cell such that it becomes larger than the surrounding cells (producing a deformation to the surrounding structure in the process). The critical point for these structures is that they were fabricated with large cladding pitches in the range of  $\Lambda = 6 \mu\text{m}$  to  $18 \mu\text{m}$  [159, 160], much larger than the  $2.8 \mu\text{m}$  or

so for the cases considered in [158]. Also with strut thicknesses down to 120nm [159] and small junction nodes, these structures are markedly different to those considered in [158]. The guidance observed within the core of these fibres is similar to that of the Kagomé fibres reported above: wide [160] and multiple [159] low-loss transmission bands, *e.g.*, the ‘single-cell #4’ fibre of [160] exhibits transmission losses below 4 dB/m over a wide spectral region from 900nm to 1600nm from a structure with a  $39\ \mu\text{m}$ – $46\ \mu\text{m}$  core diameter,  $\Lambda = 17\ \mu\text{m}$  lattice pitch and  $d = 310\text{nm}$  strut thickness.

The large-pitch square lattices, much like the large-pitch Kagomé lattices above, do not form photonic bandgaps and instead support a continuum of cladding modes, represented by the density-of-states map of [160]. Just like the Kagomé structure, the guidance mechanism is attributed to antiresonance with the lattice struts [159] with a minimal interaction between the cladding and core modes, again implying a VNW effect [160]. With this established, [160] points out that this is also the reason one observes a significant proportion of cladding light in the transmission images of the fibre endface; any light from a broad range of wavelengths coupled into the cladding can be efficiently guided there, up to the resonances of the struts as for the core modes, owing to the absence of any bandgaps.

Note that the work of [158] stated that because a full bandgap doesn’t cross the air-line for the square lattice (no junction nodes were assumed) then no core guidance could be observed. Of course, this doesn’t take into account the VNW effect and hence the work mainly concentrated on regimes in which the bandgap effect dominates. The reasons for focussing on the bandgap picture are justified in that case since the lattice pitches considered were of the order of the wavelength and significant coupling between cladding features would occur, as discussed previously. Only once the pitch is increased to larger scales do the cladding features decouple and permit the antiresonance dominated VNW guidance as observed in Ref. [160].



**Sub-Wavelength Holes** One particular guidance mechanism not yet discussed is that of *sub-wavelength guidance*: a phenomenon by which holes of diameter well below that of the wavelength of light can produce guidance with significant enhancement of the optical fields within the hole region. The basic premise of the guidance mechanism is that the fields succumb to impedance matching effects at the air/substrate boundary of the waveguide structure. As per the typical behaviour for electromagnetic waves at a dielectric interface, the fields penetrating into the low-index region (the air hole) jump in amplitude as the impedance dictates and then decay exponentially away from the interface (*e.g.*, Refs. [14] and [146]); by using a very small hole region, such as that in the core of the PCF of this paragraph’s

inset image, the fields from either side of the hole don't have enough space to decay appreciably and thus superpose to produce a significantly enhanced field than otherwise could be achieved with such small feature sizes (producing tight confinement to the sub-wavelength hole).

In the sense that it relies not on resonant interactions with cladding structure but on the evanescent decay of light within regions of low refractive index, the sub-wavelength guidance mechanism is essentially an index-guiding mechanism and does not rely on any resonant effect with the cladding (the reason it has been omitted from the comparison table below, Tables 1.1 and 1.2). Indeed, in the works discussed presently, it appears that sub-wavelength guidance requires a *finite* high-index region to surround the sub-wavelength features (giving way to a low-index outermost region) which has the effect of confining the tails of the supported modes in order to produce low-loss guidance (and likely, in order to produce any guided modes at all). This is again quite different to the resonance-based guidance mechanisms just described as the latter exist for cases where the outermost regions of the waveguide structure have a higher refractive index to the central guidance regions, not lower, and can be assumed to extend to infinity.

The sub-wavelength guidance phenomenon was first reported in theory and experiment by Wiederhecker et al. [161] using a silica PCF with a small hole, down to diameters of 110 nm, in the centre of its solid core. Scanning near-field microscope images indicated that light of particular wavelengths was indeed confined to the small hole via the described mechanism. Being able to confine light to dimensions far smaller than the wavelength has applications in scanning near-field microscopy, for example, where the collection of light from a very small region (with a large acceptance angle) is required.

The sub-wavelength guidance effect has also been applied to structures whose cores consist of an *array* of sub-wavelength holes, not just a single hole. Fibres based on this structure have been termed *porous* fibres [162–167]. Owing to the fact that the scale of the holes in which the light is guided is so small (with hole diameters of  $\sim \lambda/10$ ) most work to date has focused on the *terahertz* (THz) spectral region—also known as the *sub-millimeter wave* region:  $\lambda \approx 100\text{nm}–1\ \mu\text{m}$ ). At such long wavelengths, the waveguide structures are easier to fabricate since the features are correspondingly larger (scale invariance up to material dispersion). THz porous waveguides have been demonstrated theoretically [162–166] and experimentally [163–166]. Indeed, the work of Atakaramians et al. [162, 163] adopted the spider-web structure (discussed further in §§ 1.4 and § 2.7 and Chapter 5), initially designed for this thesis work, to the sub-wavelength hole regime. While the spider-web fibre design was initially created for the resonance-based hollow-core guidance discussed within, it was shown in Refs. [162, 163] that the structure could also guide as a porous waveguide in which the guided

light is guided within all holes of the structure (produce a Gaussian-like profile over all holes), rather than confinement predominantly to the core; this required the hole sizes to be much smaller than the wavelength (*i.e.*, hole diameter  $D_{\text{hole}} \sim \lambda/10$ ) rather than reasonably larger ( $D_{\text{hole}} \sim 10\lambda$ ) as required for the hollow-core antiresonance-based guidance it was designed for. This cross-over of the design during its development from the HC-MOF core guidance demonstrated for this thesis to that of THz porous waveguides is a result of the principal author of Refs. [162, 163] also being a member of the group I performed this thesis research within and the close relationship between the two types of waveguide regimes (just a matter of scale) and their fabrication technique (as for the spider-web fibre fabrication—Chapter 5—the porous THz waveguide employed an extrusion fabrication technique—Ref. [163]).

One of the main motivations of this type of structure for the THz regime is the ability to reduce the transmission losses to below that of the substrate material [162–166] (typically polymer for THz radiation) which, as discussed at length in the previous sections, is one of the benefits of air-guidance in general, regardless of the guidance mechanism. The porous fibre geometry has also been analysed theoretically for the optical regime for mid-IR guidance using a chalcogenide substrate [167]. Again, due to the fact that it is essentially an index-guiding mechanism with drastically different optical properties, and that it has not yet been demonstrated as a versatile HC-MOF platform, the sub-wavelength guidance mechanism does not fit within the family of low-index guiding mechanisms discussed above; needless to say, though, it clearly has merit and its own impressive qualities unattainable by other means.

### 1.3 Summary

In the preceding sections I have reviewed and discussed the current state-of-the-art hollow-core waveguides, predominantly HC-MOFs. The bias toward fibres over, say, integrated or planar waveguides is not arbitrary: MOFs are currently the only waveguide structure capable of the rich variety of structures and guidance mechanisms to which they are host to, owing to the discussed fabrication techniques possible for MOFs.

The fibres geometries discussed were based on either effectively 1-D or 2-D structures. The effectively 1-D structures discussed were the:

- Tube,
- Bragg fibre (depressed-core and the level-core ‘ARROW’ special case),
- Integrated-ARROW waveguide,
- Average-index Bragg fibre,
- and the Air-Bragg fibre.

## Effectively 1-D structures





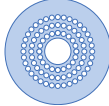
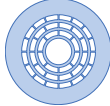
Structure	Name	Figure	Comments	Applications	Guidance
	Tube	Fig. 1.1-A	Simple structure, relatively easy to fabricate, analytic approximation ([5] and § A.4.3). High transmission loss and bend loss, highly multi-mode, poor to no dispersion control, relatively low axial modal intensity. Key publications: [5, 32, 33].	High-power CO <sub>2</sub> -laser light delivery [32, 168], dye laser transverse mode control [169], plasma induced Raman pulse amplification [170], and more.	Fresnel reflection [5]
	Bragg ( $n_{\text{core}} \leq n_0$ )	Fig. 1.1-D	Depressed-core (air/vacuum or filled), effectively 1-D multilayer cladding, cylindrical. Low loss, omnidirectional reflection (bandgaps open for all $\hat{n}$ —requires design), hollow or solid core (or liquid § 4), solid core can be small. Require compatible materials, hollow core must be large. Key publications: [10, 35–47, 63, 171, 172].	Surface-emitting fibre laser [30], sensing [19], high-power NIR/MIR delivery including precision medical surgical applications [10, 11, 41], supercontinuum generation in a small- and solid-core version [53].	Bandgap [34, 36–42] (§ 2.3)
	Bragg ( $n_{\text{core}} = n_0$ )	Fig. 1.2-A	Level-core (includes idealised air-Bragg). Requires compatible layer materials (excl. air-Bragg). Key publications: [48–51] (almost level-core [45–47, 53]).	Photonic textiles [52], supercontinuum generation in a small- and solid-core version [53] (almost level-core).	Bandgap [36, 37, 43], antiresonance [99, 173]
	Integrated-ARROW	Fig. 1.3-A,B	Planar waveguide, solid-state fabrication techniques, on-chip integrable, multiple core shapes (rectangular [57] or arch [26]). Short length, multi-mode (short length makes asymptotic single-modedness difficult [29]), restricted material choice. Key publications: [26–29, 56–59]	Microfluidics [26–29, 56, 58, 59], sensing [26, 58, 59], particle guidance and manipulation [27, 29].	Antiresonance [26, 28, 57, 61, 174]
	Average-index Bragg	Fig. 1.1-G	Single-material, effectively 1-D, effectively depressed-core (averaged ring refractive index). Requires many small cladding holes, fundamental geometrical limit to effective ring index contrast. Key publications: [63, 65, 66]	Sensing—water filled spectrum shift [67] ( <i>c.f.</i> , systematic filling of a Bragg fibre in § 4).	Bandgap [66]
	Air-Bragg	Fig. 1.1-H	Level-core, single material, large index contrast, wide low-loss transmission spectra, effectively 1-D (sans struts). Many struts required to maintain circular ring shape ( <i>c.f.</i> , my alternative polygonal spider-web fibre in § 5).	-	Bandgap [43] (idealised—§ 2), antiresonance (VNW) [9]

TABLE 1.1: Low-index core waveguides summary. Continued on Table 1.2.

## 2-D structures

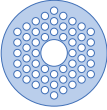

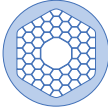
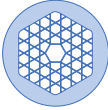


Structure	Name	Figure	Comments	Applications	Guidance
	Hexagonal (2-D)	Fig. 1.1-B	Motivated by discovery of out-of-plane bandgaps for a lattice of cylindrical holes [74, 75]. First demonstrated HC-MOF [80]. High index glasses possible exploiting novel bandgaps [76, 82, 83].	High-power ultra-short pulse compression and delivery [81].	Bandgap [34, 74, 75].
	ARROW (2-D)	Fig. 1.1-B	Typically fabricated via post-processing—filling with: liquid [102, 105–111], liquid crystal [98, 107, 109, 111, 112] or molten glass [114]. Also by directly drawing multiple glasses [96, 113] or step-index fibres inserted into a MOF [116, 117].	Refractive index sensor [102, 105–110, 112], electro-optic tunable birefringent ARROW [112], supermode MOF laser [115], various nonlinear effects [118, 119].	Antiresonance [99–102], bandgap [9, 34, 96–98, 103], PTBM [9, 98, 104]
	Honeycomb	Fig. 1.1-C	Silica. Stack-and-draw. Surface modes [81, 127–129] and their suppression [81, 128, 129]. Surface capillary wave loss minimised by tuning core wall [16, 17]: record low loss HC-MOF [17]. Bandwidth limited by max. air-filling-fraction possible [76, 82]. Other key publications: [123–126]	Nonlinear gas lasers [131], high-power soliton generation [132], other gas-based nonlinearities [133–135], electromagnetically induced transparency [136], gas sensing [137–139], particle guidance [24, 25].	Bandgap [80], PTBM [9, 104, 122, 130]
	Kagomé	Fig. 1.1-F	Variety of materials: glass, polymer. No cladding bandgaps—Bloch continuum [142, 144, 145]. Revealed photonic VNW mechanism [9, 142, 145, 150–152]. $dB/m$ level loss with only 2 [148] or 1 [149] cladding ring(s). Key publications: [9, 141–145].	Nonlinear optics: stimulated Raman scattering in H <sub>2</sub> filled fibres [141, 157], multi-octave (THz) bandwidth frequency comb generation [9, 142]. Robust integrated HC-MOF gas-cells [131]. Particle guidance [23].	Antiresonance (VNW) [9, 142, 145, 150–152]
	Square	Fig. 1.1-E	Exhibits both bandgap (for $\lambda \sim \Lambda$ ) [158] and antiresonance (via $VNW-\Lambda \gg \lambda$ ) [159] behaviour. Silica [160] and polymer [159]. Shown to withstand significant structural deformations ( <i>e.g.</i> , inflated core [159, 160]).	-	Bandgap [158], antiresonance (VNW) [159]
	Spider-web	Fig. 1.1-I	Concentric rings (annular or polygonal) with <i>colinear</i> connective struts. Presented in Chapter 5 and at ACOFT 2009 conference (awarded the Wanda Henry Prize) [175]: extruded preform with soft-glass substrate. Colinear struts $\Rightarrow$ extrusion ideal (nontrivial hole shapes). Current results indicate resonant guidance throughout visible spectrum and into NIR.	-	Antiresonance, VNW (§§ 1.4 and 5)

TABLE 1.2: Low-index core waveguides summary. Follows from Table 1.1.



The 2-D structures discussed were the:

- Hexagonal-lattice fibre,
- 2-D ARROW fibre,
- Honeycomb-lattice fibre,
- Kagomé-lattice fibre, and the
- Square-lattice fibre.

Qualitative representations of these structures were provided in Figs. 1.1, 1.2 and 1.3.

The above review of these fibres, including their associated guidance mechanisms and selected applications, is summarised in Tables 1.1 and 1.2. Due to the complex interrelations of the guidance mechanisms, many of the waveguides may or may not be able to support multiple guidance regimes (depending on their pitch, say), but only those guidance regimes which have been explicitly discussed for the specific waveguide at hand in the appropriate literature have been listed. Similarly, only the applications which were discussed above have been listed. This list is reasonably thorough, but likely not absolutely exhaustive; the motivation was to collate the majority of the most important and unique applications reported in the literature.

The rich variety of guidance mechanisms supported by the various waveguide structures was discussed. These were the:

- Bandgap effect,
- Photonic tight-binding model,
- Antiresonance, and the
- Von Neumann Wigner phenomenon.

Qualitative representations of these phenomena, how they relate to waveguidance and how they relate to each other were provided in Fig. 1.4. For completeness, these phenomena and their relationships with each other will now be summarised and reviewed briefly.

Bandgaps represent configurations of light for which Bloch modes can not exist on a given infinite optical lattice. Bloch modes exist in the allowed bands. Light incident on an infinite (half) lattice will be totally reflected if it satisfies a bandgap condition; it is transmitted if satisfying conditions within a band. A bandgap picture is a good approximation for finite periodic microstructured fibre cladding structures (for those that support bandgaps). Light within the core of such a fibre is transmitted at low loss when the bandgap conditions are satisfied (reflected from the cladding), but are attenuated rapidly (coupled out through the cladding) when the light satisfies an allowed band condition.

The photonic tight-binding model (PTBM) is simply the expression of the extreme Bloch modes whose fields are maximally bound within various structural features of the

periodic structure (the struts, apexes or holes of the honey-comb HC-MOF, say). The dispersion properties of these tightly bound Bloch modes define the edges of a given bandgap spectrum, providing a simplified means of determining bandgap spectra for waveguide design and analysis.

Antiresonance refers to a phenomenon in which light is reflected from a structural feature when it does not satisfy the guidance conditions within that feature, *e.g.*, light in the core of an ARROW fibre will be reflected from the cladding rods when it doesn't satisfy the mode conditions for the rods (examined analytically for the planar case via a reflectance analysis in this thesis—§ 3.5). Low loss modes in such a waveguide thus correspond to modes which ideally dis-satisfy the cladding rod mode condition. Light which can be guided in the cladding features is efficiently coupled out of the core, leading to large core-mode loss. Antiresonance is a practical description only when the cladding features are sufficiently decoupled from one another; otherwise the cladding features must be treated as coupled waveguides. Indeed, for fibres such as the ARROW or square-lattice fibres, bandgap guidance reduces to an antiresonance regime as the cladding pitch increases and the cladding features decouple.

The Von Neumann Wigner (VNW) phenomenon enables waveguide structures whose cladding doesn't exhibit a bandgap to support both coexisting core and cladding modes which have a minimal interaction due to a small field overlap. In this regime, antiresonance can dominate, permitting antiresonant low-loss core guidance in the absence of an equivalent bandgap behaviour.

The particulars of the aforementioned new fibre design I present in this thesis are now detailed, concluding with a summary of the thesis structure and the relationships between the various chapters.

## 1.4 Spider-Web Fibre

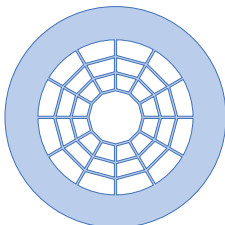


Figure 1.1-*I* qualitatively represents the fibre structure I devised, designed and fabricated during the research for this thesis. The cross sectional structure consists of concentric *polygonal* rings supported by *colinear* struts. Due to its appearance, I have coined it the *spider-web* fibre<sup>17</sup>. The fabrication and experimental results with some numerical analysis and comparison with theory of the fibre are given in Chapter 5 (with some complimentary theoretical analysis presented in § 2.7).

<sup>17</sup>I have sometimes heard this term used as a synonym for the honeycomb fibre, but its usage is rare and is clearly better suited to the structure at hand.

In general, the relative substrate layer and air gap thicknesses, the strut thicknesses, and the size of the core are arbitrary. The number of struts, hence the number points of each polygon, is also arbitrary. Due to its nature, the geometry allows *all* of these parameters to be altered independently of one another. It has similarities with the air-Bragg and Kagomé type HC-MOFs both in structure and guidance behaviour.

The primary structural difference with the air-Bragg geometry is that, instead of employing many *offset* struts in alternating air layers to support the solid concentric rings, the spider-web structure has struts which are *aligned* (colinear) with one another, and hence there are relatively fewer of them within the outermost layers compared to the air-Bragg structure, since their number must be conserved in each air layer. Because of this, surface tension effects during fabrication ensure that the concentric rings, were they to have initially been circular, adopt straight edges and thus form concentric polygons whose vertices coincide with the struts; this effect is explicitly demonstrated in the fabricated fibres presented in Chapter 5. Thus, the similarity between the spider-web and air-Bragg geometry lies in the common features of concentric rings supported by connective struts. Because of this, one would anticipate that the guidance behaviour would be similar between the two. Because the spider-web cladding is essentially a 1-D stack of substrate material and air layers, the term ‘air-Bragg’ can still apply to this structure.

The similarities with the Kagomé structure lie in the fact that the spider-web geometry consists of concentric polygons; as per Ref. [145], the Kagomé fibre guidance mechanism can be considered as that from concentric hexagons, principally due to the antiresonance or Bragg bandgap effect from the high-index rings. As discussed earlier, the addition of extra rings to the Kagomé structure appears to have little effect on decreasing the core-mode confinement loss [145]. Thus, as suggested earlier, by removing as many struts as possible, this excessive tunneling effect may be circumvented. By reducing the structure to concentric hexagons supported only by colinear struts coincident with the polygon vertices, the resonant influence of the concentric polygons could potentially overcome this tunneling through the struts. This concept is embodied in the spider-web structure by design.

In this sense, the spider-web HC-MOF design lies somewhere between the air-Bragg and Kagomé designs. It embodies the ideal of concentric rings suspended in air (*c.f.*, quotation of Prof. Russell above) and represents a fabricable version of the idealised, concentric polygon, version of the Kagomé fibre geometry of Ref. [145].

Important to both of these structural comparisons is that the air-filling fraction in all cases is reasonably large with a large lattice pitch (compared to the guided light wavelength), *i.e.*, all structural features such as struts and rings are relatively thin and well

separated. To draw the point a final time, the guidance phenomena of other large-pitch structures such as the air-Bragg and Kagomé fibres above would thus be expected to translate to the spider-web geometry here, including antiresonance in the presence of Von Neumann Wigner cladding mode continuum coexistence phenomena.

## 1.5 Thesis Structure

This thesis is structured in a manner representing both a logical evolution of the ideas embodied in each chapter and also a relatively close chronology of the results as they were completed.

Chapter 2 discusses the principles behind the guidance of level-core Bragg fibres, with an emphasis towards silica air-Bragg fibres. Higher-order bandgaps in such waveguides are investigated numerically, finding that higher order gaps typically exhibit much lower modal confinement loss, at the expense of bandwidth. Exploitation of this phenomenon for reducing confinement loss at a given wavelength is demonstrated; it is shown that, at least for low-order modes, increasing the scale of the entire fibre geometry in order to shift a low-loss higher-order gap to a particular wavelength is far more practical than increasing the core size in order to achieve an equivalent reduction in confinement loss for that wavelength. The chapter also discusses some fundamental properties of the guidance behaviour of level-core Bragg fibres, such as the relationship of the guided core modes' dispersive behaviour to that of a dielectric tube.

Chapter 3 naturally follows in that the spectral properties for general depressed-core Bragg waveguides are explored. In doing so, an intimate relationship between the bandgap and anti-resonance guidance mechanisms is examined. In identifying this relationship, and from it a simple, analytic, antiresonance model describing confinement of light on or *below* the light-line of the lowest layer material index is derived and coined the *Stratified Planar Anti-Resonant Reflecting Optical Waveguide* (SPARROW) model. The implications of the SPARROW model are then discussed with its efficacy in determining a waveguide's spectral transmission regions demonstrated via the numerical modelling of a full Bragg fibre structure whose core has been filled with an index between that of the lowest cladding layer and vacuum. The SPARROW model is also extended to demonstrate how it can be applied to the description of nontrivial properties of the full 2-D bandgap spectra of such 1-D photonic crystal structures, such as: a consistent nomenclature for arbitrary bandgap spectra; the approximate position of lowest core-mode confinement loss of any gap; the precise closure points of a given gap; the center of a gap in both bandgap map dimensions (not just in wavelength); and the number of

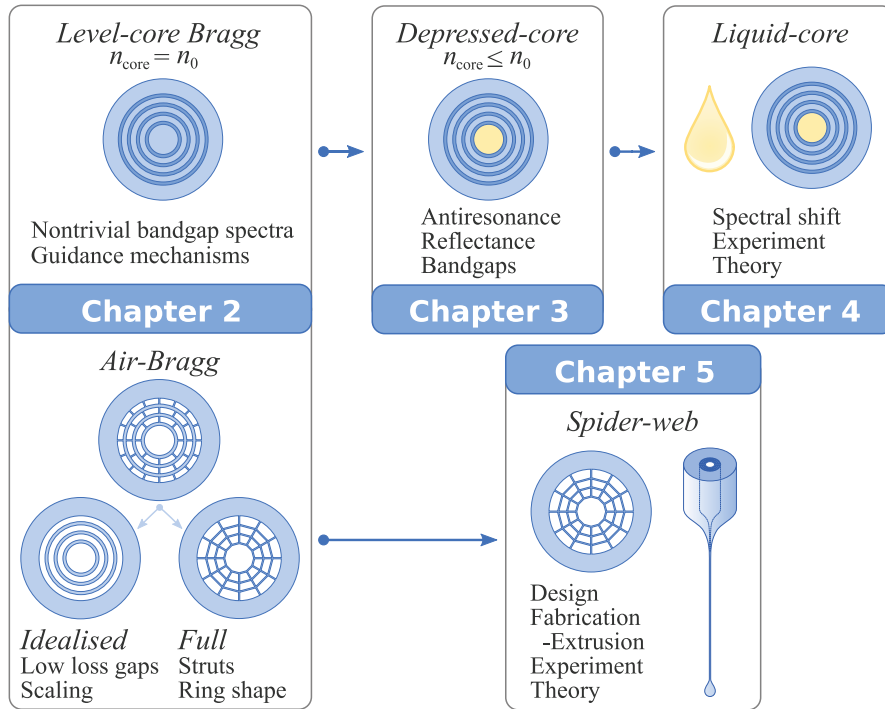


FIGURE 1.8: Relational diagram of the main chapters, reflecting the relationship between the principal themes of each chapter. There are of course many other fundamental and subtle relationships between the sections not depicted in the figure.

bandgaps within a specific domain, thus describing the bandgap spectrum topology; all via simple analytic expressions.

Chapter 4 discusses the experimental results of systematically filling a Bragg fibre with liquids of various refractive indices. The refractive index of the core is shown to dictate which region of the layered cladding's 2-D bandgap spectrum is intercepted by the lowest-loss guided modes. The transmission spectrum is shown to be shifted to lower wavelengths as the core index is increased. The results are directly compared with theoretical predictions based on the cladding bandgap spectrum with convincing agreement between the two.

Chapter 5 presents the design, fabrication and experimental demonstration of a novel hollow-core microstructured optical fibre made from *soft-glass* via an *extrusion* preform fabrication technique. As discussed above, the structure for this fibre was chosen to be an air-Bragg fibre structure whose cross-section is reminiscent of a spider-web. Insight into the guidance behaviour of the fabricated 2-ring spider-web fibre of Chapter 5 is given by considering antiresonance, reflectance and modal pictures using a variety of modelling techniques.

Appendix A gives a comprehensive review of the theory relevant to this thesis. It contains the results from the relevant literature reformulated and re-derived for the present

work; many of the steps that are glossed over in the literature have been explicitly demonstrated for completeness. This is done in the hope that the concepts and conventions used within are explicit and obvious—something that otherwise requires some effort when consulting multiple references.

Appendix B provides a reference to miscellaneous mathematical concepts and identities, with derivations where appropriate. These are referenced either in the main text or, more frequently, in the theory of Appendix A.

Figure 1.8 depicts a relational map between the chapters. Chapters 2  $\rightarrow$  3  $\rightarrow$  4 are connected in that they follow the conceptual path of: *level-core theory*  $\rightarrow$  *depressed-core theory*  $\rightarrow$  *depressed-core experiment*. Chapters 2  $\rightarrow$  5 are conceptually related as: *air-Bragg and polygonal ring theory*  $\rightarrow$  *fabrication and numerical analysis of spider-web fibres*.

## 1.6 Concluding Remarks

The myriad guidance mechanisms displayed by the vast variations of structures of low-index guiding waveguides has been reviewed. Fundamental waveguidance concepts have been highlighted and explained throughout, albeit mostly qualitatively. It is clear that the versatility of low-index guiding waveguides (especially those with a hollow-core) makes them ideal for varied applications such as high-power delivery, gas-based highly nonlinear photonics, fibre lasers (nonlinear and gain-media based), frequency comb generation for atto-science and metrology, sensing (*e.g.*, refractive index, temperature), medicine (surgery), and more. The reviewed waveguides, their properties, applications and guidance mechanisms were collated in Tables 1.1 and 1.2. The guidance mechanisms themselves, and their relationships to each other, were summarised in Fig. 1.7.

The following chapters (summarised in § 1.5) will discuss various findings relating to low-index guiding waveguides including: theoretical analysis of higher-order bandgaps in idealised air-Bragg fibres and the influence of cladding ring shape and strut incorporation and configuration; generalising the antiresonance concept to depressed-core waveguides; experimental analysis of the spectral properties of liquid filled Bragg fibres; and the design, fabrication and theoretical analysis of a novel HC-MOF—the spider-web fibre.

